

# Effects of mixing with quark singlets

J. A. Aguilar–Saavedra

*Departamento de Física and Grupo de Física de Partículas (GFP),  
Instituto Superior Técnico, P-1049-001 Lisboa, Portugal*

## Abstract

The mixing of the known quarks with new heavy singlets can modify significantly some observables with respect to the Standard Model predictions. We analyse the range of deviations permitted by the constraints from precision electroweak data and flavour-changing neutral processes at low energies. We study top charged current and neutral current couplings, which will be directly tested at top factories, like LHC and TESLA. We discuss some examples of observables from  $K$  and  $B$  physics, as the branching ratio of  $K_L \rightarrow \pi^0 \nu \bar{\nu}$ , the  $B_s^0$  mass difference or the time-dependent CP asymmetry in  $B_s^0 \rightarrow D_s^+ D_s^-$ , which can also show large new effects.

## 1 Introduction

The successful operation of LEP and SLD in the past few years has provided precise experimental data [1, 2] with which the Standard Model (SM) and its proposed extensions must be confronted. The results for  $\varepsilon'/\varepsilon$  have converged [3, 4], providing evidence for direct CP violation in the neutral kaon system. In addition,  $B$  factories have begun producing data on  $B$  decays and CP violation, which test the Cabibbo-Kobayashi-Maskawa (CKM) matrix elements involving the top quark and the CKM phase  $\delta$ . However, the determination of most parameters involving the top quark is still strongly model-dependent. While the CKM matrix elements that mix light quarks are extracted from tree-level processes (and hence their measurement is model-independent to a large extent), the charged current couplings  $V_{td}$  and  $V_{ts}$  are derived from one-loop processes [5], to which new physics beyond the SM may well contribute. The Tevatron determination of  $V_{tb}$  in top pair production [6] is obtained assuming  $3 \times 3$  CKM unitarity, and the neutral current interactions of the top with the  $Z$  boson remain virtually unknown from the experimental point of view. This fact contrasts with the high

precision achieved for the couplings of the  $b$  and  $c$  quarks at LEP and SLD, obtained from the ratios  $R_b$ ,  $R_c$  and the forward-backward (FB) asymmetries  $A_{\text{FB}}^{0,b}$ ,  $A_{\text{FB}}^{0,c}$ .

The situation concerning CP violating phases is better (see for instance Ref. [7, 8]). Few years ago, the single phase  $\delta$  present in the CKM matrix could merely be adjusted to reproduce the experimental value of the only CP violation observable available,  $\varepsilon$  in the kaon system. With the resolution of the conflict between the NA31 and E731 values of  $\varepsilon'/\varepsilon$ , and the recent measurement of the CP asymmetry  $a_{\psi K_S}$  in the  $B$  system [9, 10], there are two new CP violation observables, both in agreement with the SM predictions, which allow to test the CKM picture of CP violation. Experiments under way at  $B$  factories keep investigating other CP asymmetries to dig out the phase structure of the CKM matrix. Likewise, the knowledge of the top quark properties will improve in the next years, with the arrival of top factories, LHC and TESLA [11, 12]. For instance, single top production at LHC [13, 14, 15] will yield a measurement of  $V_{tb}$  with an accuracy of  $\pm 7\%$ . In top pair production, the angular distributions of the top decay products will provide a very precise determination of the structure of the  $Wtb$  vertex, even sensitive to QCD corrections [16]. The prospects for  $V_{td}$  and  $V_{ts}$  are less optimistic due to the difficulty in tagging the light quark jets.

Before top factories come into operation, it is natural to ask ourselves how large the departures from the SM predictions might be. Answering this question means knowing how precisely one can indirectly fix the allowed values of the least known parameters, taking into account all the present relevant data from electroweak precision measurements and from kaon,  $D$  and  $B$  physics. We will show that there is still large room for new physics, which may manifest itself in the form of deviations of the properties of the known quarks from SM expectations. This is especially the case for the top quark, whose couplings are poorly known, and also for rare  $K$  decays and CP asymmetries in the  $B$  systems, which are currently being probed at  $K$  and  $B$  factories.

With this aim we study a class of SM extensions in which  $Q = 2/3$  up-type or  $Q = -1/3$  down-type quark singlets are added to the three SM families [17, 18, 19, 20, 21, 22, 23, 24, 25, 26, 27]. These exotic quarks, often called vector-like, have both their left and right components transforming as singlets under  $SU(2)_L$ , and therefore their addition to the SM quark content does not spoil the cancellation of the triangle anomalies. In these models, which are described in the next Section,  $3 \times 3$  CKM unitarity does not necessarily hold, and mixing of the new quarks with the standard ones can lead to sizeable departures from the SM predictions [28, 29, 30, 31]. For instance, the CKM matrix elements  $V_{td}$ ,  $V_{ts}$  and  $V_{tb}$  and the top neutral current couplings with the  $Z$  boson

can be quite different from SM expectations. The ratio of branching fractions of the “golden modes”  $\text{Br}(K_L \rightarrow \pi^0 \nu \bar{\nu})/\text{Br}(K^+ \rightarrow \pi^+ \nu \bar{\nu})$  can have an enhancement of one order of magnitude with respect to the SM prediction, and the time-dependent CP asymmetry in the decay  $B_s^0 \rightarrow D_s^+ D_s^-$ , which is predicted to be very small in the SM, can vary between  $-0.4$  and  $0.4$ .

Apart from their simplicity and the potentially large effects on experimental observables, there are several theoretical reasons to consider quark isosinglets. Down singlets appear in grand unification theories [22, 32, 33], for instance those based on the gauge group  $E_6$  (in the 27 representation of  $E_6$  a  $Q = -1/3$  singlet is associated to each fermion family). The presence of down singlets does not spoil gauge coupling unification, as long as they are embedded within the 27 representation of  $E_6$  [25, 26]. When added to the SM particle content, they can improve the convergence of the couplings, but not as well as in the minimal supersymmetric SM [34]. Models with large extra dimensions with for instance  $t_R$  in the bulk predict the existence of a tower of  $Q = 2/3$  singlets  $T_{L,R}^{(n)}$ . If there is multilocalisation the lightest one,  $T_{L,R}^{(1)}$ , can have a mass  $m_T \sim 300$  GeV or larger and an observable mixing with the top [35]. Similarly, if  $b_R$  is in the bulk, there exists a tower of  $B_{L,R}^{(n)}$ , but the mixing with SM fermions is suppressed in relation to the top case if the Higgs is restricted to live on the boundary.

There are three recent studies regarding the constraints on models with extra singlets [36, 37, 38]. In this work, we extend these analyses in three main aspects: *(i)* We include up singlets, as well as down singlets, referring to them as Model I and II, respectively. *(ii)* We study the limits on  $V_{td}$ ,  $V_{ts}$ ,  $V_{tb}$ , top neutral current couplings and other observables not previously analysed; *(iii)* We take a larger set of experimental constraints into account: the correlated measurement of  $R_b$ ,  $R_c$ ,  $A_{\text{FB}}^{0,b}$ ,  $A_{\text{FB}}^{0,c}$ ,  $\mathcal{A}_b$ ,  $\mathcal{A}_c$ ; oblique corrections; the  $|\delta m_B|$ ,  $|\delta m_{B_s}|$  and  $|\delta m_D|$  mass differences; the CP violation observables  $\varepsilon$ ,  $\varepsilon'/\varepsilon$ ,  $a_{\psi_{K_S}}$ ; the decays  $b \rightarrow s \gamma$ ,  $b \rightarrow s \mu^+ \mu^-$ ,  $b \rightarrow s e^+ e^-$ ,  $K^+ \rightarrow \pi^+ \nu \bar{\nu}$  and  $K_L \rightarrow \mu^+ \mu^-$ ;  $\nu N$  processes and atomic parity violation. In addition, we examine several other potential restrictions, which turn out to be less important than the previous ones. We allow mixing of all the generations with either  $Q = 2/3$  or  $Q = -1/3$  exotic quarks, and we consider that one or two singlets can mix significantly, though for brevity in the notation we always refer to one extra singlet  $T$  or  $B$ .

This paper is organised as follows: In Section 2 the main features of the models are described. In Section 3 we summarise the direct limits on CKM matrix elements and the masses of the new quarks. In Section 4 we review the constraints from precision electroweak data:  $R_b$ ,  $R_c$ , asymmetries and oblique corrections. In Section 5 we focus

our attention on flavour-changing neutral (FCN) processes at low energies: meson mixing,  $B$  decays and kaon decays. The various constraints on the  $Z$  couplings of the  $u$ ,  $d$  quarks are studied in Section 6. We introduce the formalism necessary for the discussion of some observables from  $K$  and  $B$  physics in Section 7. We present the results in Section 8, and in Section 9 we draw our conclusions. In Appendix A we collect the common input parameters for our calculations, and in Appendix B the Inami-Lim functions needed. The statistical prescriptions used in our analysis are explained in Appendix C.

## 2 Brief description of the models

In order to fix our notation briefly, in this Section we will be a little more general than needed in the rest of the paper (see for instance Ref. [39] for an extended discussion including isodoublets and mirror quarks too). We consider a SM extension with  $N$  standard quark families and  $n_u$  up,  $n_d$  down vector-like singlets. The total numbers of up and down quarks,  $\mathcal{N}_u = N + n_u$  and  $\mathcal{N}_d = N + n_d$ , respectively, are not necessarily equal. In these models, the charged and neutral current terms of the Lagrangian in the weak eigenstate basis can be written in matrix notation as

$$\begin{aligned}\mathcal{L}_W &= -\frac{g}{\sqrt{2}} \bar{u}_L^{(d)} \gamma^\mu d_L^{(d)} W_\mu^+ + \text{h.c.}, \\ \mathcal{L}_Z &= -\frac{g}{2c_W} \left( \bar{u}_L^{(d)} \gamma^\mu u_L^{(d)} - \bar{d}_L^{(d)} \gamma^\mu d_L^{(d)} - 2s_W^2 J_{\text{EM}}^\mu \right) Z_\mu,\end{aligned}\tag{1}$$

with  $(u_L^{(d)}, d_L^{(d)})$  doublets under  $\text{SU}(2)_L$  of dimension  $N$  in flavour space. These terms have the same structure as in the SM, with  $N$  generations of left-handed doublets in the isospin-related terms, but with all the  $\mathcal{N}_u, \mathcal{N}_d$  fields in  $J_{\text{EM}}^\mu$ . The differences show up in the mass eigenstate basis, where the Lagrangian reads

$$\begin{aligned}\mathcal{L}_W &= -\frac{g}{\sqrt{2}} \bar{u}_L \gamma^\mu V d_L W_\mu^+ + \text{h.c.}, \\ \mathcal{L}_Z &= -\frac{g}{2c_W} \left( \bar{u}_L \gamma^\mu X^u u_L - \bar{d}_L \gamma^\mu X^d d_L - 2s_W^2 J_{\text{EM}}^\mu \right) Z_\mu.\end{aligned}\tag{2}$$

Here  $u = (u, c, t, T, \dots)$  and  $d = (d, s, b, B, \dots)$  are  $\mathcal{N}_u$  and  $\mathcal{N}_d$  dimensional vectors, and  $X^u, X^d$  are matrices of dimension  $\mathcal{N}_u \times \mathcal{N}_u, \mathcal{N}_d \times \mathcal{N}_d$ , respectively. In general the  $\mathcal{N}_u \times \mathcal{N}_d$  CKM matrix  $V$  is neither unitary nor square.

The most distinctive feature of this class of models is the appearance of tree-level FCN couplings in the mass eigenstate basis, originated by the mixing of weak eigen-

states with the same chirality and different isospin. These FCN interactions mix left-handed fields, and are determined by the off-diagonal entries in the matrices  $X^u$ ,  $X^d$ . On the other hand, the diagonal  $Zqq$  terms of up- or down-type mass eigenstates  $q$  are (dropping here the superscript on the  $X$  matrices)

$$\begin{aligned} c_L^q &= \pm X_{qq} - 2Q_q s_W^2, \\ c_R^q &= -2Q_q s_W^2, \end{aligned} \quad (3)$$

with the plus (minus) sign for up (down) quarks. With these definitions, the flavour-diagonal  $Zqq$  vertices read

$$\mathcal{L}_{Zqq} = -\frac{g}{2c_W} (\bar{q}\gamma^\mu c_L^q q_L + \bar{q}_R\gamma^\mu c_R^q q_R). \quad (4)$$

For a SM-like mass eigenstate without any left-handed singlet component,  $X_{qq} = 1$ ,  $X_{qq'} = 0$  for  $q' \neq q$ , and it has standard interactions with the  $Z$  boson. For a mass eigenstate with singlet components,  $0 < X_{qq} < 1$ , what implies nonzero FCN couplings  $X_{qq'}$  as well.

Let us write the unitary transformations between the mass and weak interaction eigenstates,

$$\begin{aligned} u_L^0 &= \mathcal{U}^{uL} u_L, & u_R^0 &= \mathcal{U}^{uR} u_R, \\ d_L^0 &= \mathcal{U}^{dL} d_L, & d_R^0 &= \mathcal{U}^{dR} d_R, \end{aligned} \quad (5)$$

where  $\mathcal{U}^{qL}$  and  $\mathcal{U}^{qR}$  are  $\mathcal{N}_q \times \mathcal{N}_q$  unitary matrices. The weak interaction eigenstates  $q_{L,R}^0$  include doublets and singlets. It follows from Eqs. (1,2) that

$$\begin{aligned} V_{\alpha\sigma} &= (\mathcal{U}_{i\alpha}^{uL})^* \mathcal{U}_{i\sigma}^{dL}, \\ X_{\alpha\beta}^u &= (\mathcal{U}_{i\alpha}^{uL})^* \mathcal{U}_{i\beta}^{uL}, & X_{\sigma\tau}^d &= (\mathcal{U}_{j\sigma}^{dL})^* \mathcal{U}_{j\tau}^{dL} \end{aligned} \quad (6)$$

with  $i, j$  running over the left-handed doublets,  $\alpha, \beta = u, c, t, T, \dots$  and  $\sigma, \tau = d, s, b, B, \dots$ . From these equations it is straightforward to obtain the relations

$$\begin{aligned} X^u &= V V^\dagger, \\ X^d &= V^\dagger V, \end{aligned} \quad (7)$$

and to observe that  $X^u = (X^u)^\dagger$ ,  $X^d = (X^d)^\dagger$ . Furthermore, we can see that in general  $V$  is not an unitary matrix. We will restrict our discussion to models where either  $n_d = 0$  or  $n_u = 0$ , *i. e.* we will consider either up singlets or down singlets, but not

both at the same time. In this context  $V$  is a submatrix of a unitary matrix, and in each case we can write

$$\begin{aligned} X_{\alpha\beta}^u &= \sum_{i=1}^N V_{\alpha i} V_{\beta i}^* = \delta_{\alpha\beta} - \sum_{i=N+1}^{\mathcal{N}_u} V_{\alpha i} V_{\beta i}^*, \\ X_{\sigma\tau}^d &= \sum_{i=1}^N V_{i\sigma}^* V_{i\tau} = \delta_{\sigma\tau} - \sum_{i=N+1}^{\mathcal{N}_d} V_{i\sigma}^* V_{i\tau}. \end{aligned} \quad (8)$$

It is enlightening to observe that for  $\alpha \neq \beta$ ,  $\sigma \neq \tau$ , we have the inequalities [39, 40]

$$\begin{aligned} |X_{\alpha\beta}^u|^2 &\leq (1 - X_{\alpha\alpha}^u)(1 - X_{\beta\beta}^u), \\ |X_{\sigma\tau}^d|^2 &\leq (1 - X_{\sigma\sigma}^d)(1 - X_{\tau\tau}^d). \end{aligned} \quad (9)$$

Therefore, if for instance  $X_{\alpha\alpha}^u = 1$  (that is, if the diagonal  $Z$  vertex is the same as in the SM) the off-diagonal couplings involving the quark  $\alpha$  vanish. As a rule of thumb, FCN couplings arise at the expense of decreasing the diagonal ones. This fact has strong implications on the limits on FCN couplings, as we will later see.

The equality for  $X^u$  in Eq. (9) holds in particular if  $n_u = 1$ . Likewise, the equality for  $X^d$  holds when  $n_d = 1$ . This implies that the introduction of *only one* extra singlet mixing significantly (as it is usually done in the literature) results in additional restrictions in the parameter space, and in principle may lead to different predictions. Moreover, for  $n_u = 1$  or  $n_d = 1$  the CKM matrix has three independent CP violating phases, whereas for  $n_u = 2$  or  $n_d = 2$  there are five. Hence, in our numerical analysis we will consider also the situation when two singlets can have large mixing,  $n_u = 2$ ,  $n_d = 0$  or  $n_u = 0$ ,  $n_d = 2$ , to give a more complete picture. In the rest of the paper we write the expressions for only one extra singlet for simplicity.

### 3 Direct limits

Even though in these SM extensions the  $3 \times 3$  CKM matrix is not unitary, in the two examples under study it is still a submatrix of a  $4 \times 4$  unitary matrix  $V$ . The direct determination of the moduli of CKM matrix elements [5] in Table 1 not only sets direct limits on these CKM elements themselves but also unitarity bounds on the rest. After the requirement of  $V_{tb} \sim 1$  from precision electroweak data (see Section 4) these bounds are stronger. In this case, the Tevatron constraint [6]

$$\frac{|V_{tb}|^2}{|V_{td}|^2 + |V_{ts}|^2 + |V_{tb}|^2} = 0.97_{-0.24}^{+0.31} \quad (10)$$

$ V_{ud} $	$0.9735 \pm 0.0008$
$ V_{us} $	$0.2196 \pm 0.0023$
$ V_{ub} $	$(3.6 \pm 1.0) \times 10^{-3}$
$ V_{cd} $	$0.224 \pm 0.016$
$ V_{cs} $	$0.97 \pm 0.11$
$ V_{cb} $	$0.0402 \pm 0.0019$

Table 1: Direct measurements of CKM matrix elements.  $V_{ub}$  is obtained from  $|V_{cb}|$  and the ratio  $|V_{ub}/V_{cb}|$ .

is automatically satisfied.

The non-observation of top decays  $t \rightarrow qZ$ ,  $q = u, c$  at Tevatron [41] provided the first limit on FCN couplings involving the top,  $|X_{qt}| \leq 0.84$  (from now on we omit the superscript when it is obvious). These figures have improved with the analysis of single top production at LEP in the process  $e^+e^- \rightarrow t\bar{q} + \bar{t}q$ , which sets the bounds  $|X_{qt}| \leq 0.41$  [42]. LEP limits are model-dependent because in single top production there might possibly be contributions from a  $\gamma tq$  effective coupling. These vertices are very small in most SM extensions, in particular in models with quark singlets [43], thus in our case the photon contribution may be safely ignored.

As long as new quarks have not been observed at Tevatron nor LEP, there are various direct limits on their masses, depending on the decay channel analysed [5]. We assume  $m_T, m_B > 200$  GeV in our evaluations.

## 4 Limits from precision electroweak data

### 4.1 $R_b, R_c$ and FB asymmetries

In the discussion after Eqs. (9) we have observed that FCN interactions can be bounded by examining the deviation from unity of the diagonal ones. This is a particular example of a more general feature of these models, that the isosinglet component of a mass eigenstate can be determined from its diagonal couplings with the  $Z$  boson. In this Section we will explain how the experimental knowledge of  $R_b, R_c$  and the FB asymmetries of the  $b$  and  $c$  quarks constrains their mixing with isosinglets. We will study in detail the case of the bottom quark; the discussion for the charm is rather

alike.

$R_b$  is defined as the ratio

$$R_b = \frac{\Gamma(Z \rightarrow b\bar{b})}{\Gamma(Z \rightarrow \text{hadrons})}. \quad (11)$$

The partial width to hadrons includes  $u\bar{u}$ ,  $d\bar{d}$ ,  $s\bar{s}$ ,  $c\bar{c}$  and  $b\bar{b}$ . The numerator of this expression is proportional to  $(c_L^b)^2 + (c_R^b)^2$  plus a smaller term proportional to  $m_b$ . The pole FB asymmetry of the  $b$  quark is defined as

$$A_{\text{FB}}^{0,b} = \frac{\sigma(\cos\theta > 0) - \sigma(\cos\theta < 0)}{\sigma(\cos\theta > 0) + \sigma(\cos\theta < 0)}, \quad (12)$$

where  $\theta$  is the angle between the bottom and the electron momenta in the centre of mass frame <sup>1</sup>. The coupling parameter  $\mathcal{A}_b$  of the bottom is defined as

$$\mathcal{A}_b = \frac{(c_L^b)^2 - (c_R^b)^2}{(c_L^b)^2 + (c_R^b)^2}. \quad (13)$$

It is obtained from the left-right-forward-backward asymmetry of the  $b$  quark at SLD, and considered as an independent parameter in the fits, despite the fact that the FB asymmetry can be expressed as  $A_{\text{FB}}^{0,b} = 3/4 \mathcal{A}_e \mathcal{A}_b$ , with  $\mathcal{A}_e$  the coupling parameter of the electron.

At tree-level,  $c_L^b = -X_{bb} + 2/3s_W^2$ ,  $c_R^b = 2/3s_W^2$ , hence in a first approximation the mixing of the  $b$  quark with down singlets in Model II decreases  $X_{bb}$  from unity and thus decreases  $R_b$ ,  $\mathcal{A}_b$  and  $A_{\text{FB}}^{0,b}$ . The effect of some electroweak radiative corrections can be taken into account using an  $\overline{\text{MS}}$  definition of the sine of the weak angle,  $s_Z^2 = 0.23113$  [5] and for the electron coupling an “effective” leptonic  $\sin^2\theta_{\text{lept}}^{\text{eff}} = 0.23137$  [1]. Other electroweak and QCD corrections that cannot be absorbed into these definitions are included as well [44, 45]. They are of order 0.6% for  $u$ ,  $c$  and  $-0.25\%$  for  $d$ ,  $s$ ,  $b$ . Furthermore, for the bottom quark there is an important correction originated by triangle diagrams involving the top [46]:

$$\delta c_L^b = 2 \left( \frac{\alpha}{2\pi} \right) |V_{tb}|^2 F(x_t) \quad (14)$$

(note that we use a different normalisation with respect to Ref. [46]), with  $x_t = (m_t/M_W)^2$  and

$$F(x_t) = \frac{1}{8s_W^2} [x_t + 2.880 \log x_t - 6.716 + (8.368 \log x_t - 3.408)/x_t + (9.126 \log x_t + 2.260)/x_t^2 + (4.043 \log x_t + 7.410)/x_t^3 + \dots]. \quad (15)$$

---

<sup>1</sup>These two observables *do not* include the photon contributions, and  $A_{\text{FB}}^{0,b}$  is defined for massless external particles. They are extracted from the experimental measurement of  $e^+e^- \rightarrow b\bar{b}$  after correcting for the photon contribution, external masses and other effects [1, 2].



We have omitted the imaginary part of  $F(x_t)$  since it does not contribute to  $\delta c_L^b$ . This large correction  $\sim (m_t/M_W)^2$  is a consequence of the non-decoupling behaviour of the top quark, and CKM suppression makes it relevant only for the bottom. It decreases the value of  $R_b$  by  $4\sigma$  and has the indirect effect of increasing  $R_c$  slightly. Its inclusion is then crucial to compare the theoretical calculation with experiment. In Table 2 we collect our SM predictions for  $R_b$ ,  $R_c$ ,  $A_{\text{FB}}^{0,b}$ ,  $A_{\text{FB}}^{0,c}$ ,  $\mathcal{A}_b$  and  $\mathcal{A}_c$  calculated using the parameters in Appendix A, together with the experimental values found in Ref. [1]. The masses used are  $\overline{\text{MS}}$  masses at the scale  $M_Z$ . The correlation matrix necessary for the fit is in Table 3.

	SM prediction	Experimental measurement	Total error
$R_b$	0.21558	0.21646	0.00065
$R_c$	0.1722	0.1719	0.0031
$A_{\text{FB}}^{0,b}$	0.1039	0.0990	0.0017
$A_{\text{FB}}^{0,c}$	0.0744	0.0685	0.0034
$\mathcal{A}_b$	0.935	0.922	0.020
$\mathcal{A}_c$	0.669	0.670	0.026

Table 2: SM calculation of  $R_b$ ,  $R_c$ ,  $A_{\text{FB}}^{0,b}$ ,  $A_{\text{FB}}^{0,c}$ ,  $\mathcal{A}_b$ ,  $\mathcal{A}_c$  and experimental values.

	$R_b$	$R_c$	$A_{\text{FB}}^{0,b}$	$A_{\text{FB}}^{0,c}$	$\mathcal{A}_b$	$\mathcal{A}_c$
$R_b$	1.00	-0.14	-0.08	0.01	-0.08	0.04
$R_c$	-0.14	1.00	0.04	-0.01	0.03	-0.05
$A_{\text{FB}}^{0,b}$	-0.08	0.04	1.00	0.15	0.02	0.00
$A_{\text{FB}}^{0,c}$	0.01	-0.01	0.15	1.00	0.00	0.01
$\mathcal{A}_b$	-0.08	0.03	0.02	0.00	1.00	0.13
$\mathcal{A}_c$	0.04	-0.05	0.00	0.01	0.13	1.00

Table 3: Correlation matrix for the experimental measurements of  $R_b$ ,  $R_c$ ,  $A_{\text{FB}}^{0,b}$ ,  $A_{\text{FB}}^{0,c}$ ,  $\mathcal{A}_b$  and  $\mathcal{A}_c$ .

The mixing of the  $b$  quark with down isosinglets decreases  $V_{tb}$ , making this negative correction smaller in modulus. This is however less important than the effect of the deviation of  $X_{bb}$  from unity. The net effect is that in Model II  $X_{bb}$ , and hence also  $V_{tb}$ , are tightly constrained by  $R_b$  to be very close to unity.

In Model I the mixing of the top with singlets modifies the  $Ztt$  interactions, and the expression for  $\delta c_L^b$  in Eq. (14) must be corrected accordingly (see Ref. [47] and also Ref. [48]). The decrease in  $X_{tt}$  can be taken into account with the substitution  $F \rightarrow F + F_2$ , with

$$F_2(x_t) = \frac{1}{8s_W^2} \frac{X_{tt} - 1}{2} x_t \left( 2 - \frac{4}{x_t - 1} \log x_t \right). \quad (16)$$

Moreover, there are additional triangle diagrams with the mass eigenstate  $T$  replacing the top, or involving  $t$  and  $T$ . The  $T$  quark contribution is added to Eq. (14) as the top term but multiplied by  $|V_{Tb}|^2$ . The  $t - T$  contribution is given by  $V_{tb}^* V_{Tb} F_3(x_t, x_T)$ , with  $x_T = (m_T/M_W)^2$  and <sup>2</sup>

$$F_3(x_t, x_T) = \frac{1}{2s_W^2} \frac{\text{Re } X_{tT}}{2} \left[ -\frac{1}{x_T - x_t} \left( \frac{x_T^2}{x_T - 1} \log x_T - \frac{x_t^2}{x_t - 1} \log x_t \right) + \frac{x_t x_T}{x_T - x_t} \left( \frac{x_T}{x_T - 1} \log x_T - \frac{x_t}{x_t - 1} \log x_t \right) \right]. \quad (17)$$

In Model I this radiative correction gives the leading effect on  $R_b$  of the mixing. However, the presence of the new quark may make up for the difference in the top contribution. Should the new mass eigenstate be degenerate with the top,  $m_T = m_t$  and  $x_T = x_t$ , one can verify that

$$|V_{tb}|^2 F(x_t) + |V_{Tb}|^2 F(x_T) = |V_{tb}|^2 [F(x_t) + F_2(x_t)] + |V_{Tb}|^2 [F(x_T) + F_2(x_T)] + V_{tb}^* V_{Tb} F_3(x_t, x_T), \quad (18)$$

as intuitively might be expected. Since  $(|V_{tb}|^2 + |V_{Tb}|^2) = |V_{tb}|_{\text{SM}}^2$ , this means that for degenerate  $t, T$  the correction has the same value as in the SM (and in this situation the terms with  $F_2$  and  $F_3$  cancel each other). For  $m_T \sim m_t$ ,  $\delta c_L^b$  has a similar magnitude as in the SM and low values  $V_{tb} \sim 0.6$  are allowed. For heavier  $T$ , the size of this radiative correction sets limits on the CKM angle  $V_{Tb}$ , and thus on  $V_{tb}$ .

The study of the charm mixing and the constraints on its couplings from  $R_c$ ,  $\mathcal{A}_c$  and  $A_{\text{FB}}^{0,c}$  is completely analogous (interchanging the rôle of up and down singlets). In principle, the presence of a new heavy down quark  $B$  induces a large  $m_B^2$ -dependent correction, but this is suppressed by the CKM factor  $|V_{cB}|^2$  and hence the analysis is simplified. The pole FB asymmetry of the quark  $s$  has also been measured recently,

---

<sup>2</sup>In obtaining Eq. (17) from the results quoted in Ref. [46] we have assumed a CKM parameterisation with  $V_{tb}^* V_{Tb}$  real. This is our case with the parameterisations used in the numerical analysis in Section 8.

$A_{\text{FB}}^{0,s} = 0.1008 \pm 0.0120$  [49], though not nearly with the same precision as the  $b$  and  $c$  asymmetries. This determination assumes that the FB asymmetries of the  $u, d$  quarks and the  $Z$  branching ratios are fixed at their SM values and thus cannot be properly taken as a direct measurement. We do not include it as a constraint, but anyway we have checked that at this level of experimental precision it would not provide any additional constraint on the model.

## 4.2 Oblique parameters

The oblique parameters  $S$ ,  $T$  and  $U$  [50, 51] are used to summarise the effects of new particles in weak currents in a compact form. Provided these particles are heavy and couple weakly to the known fermions, their leading effects in processes with only SM external particles are radiative corrections given by vacuum polarization diagrams (oblique corrections), rather than triangle and box diagrams (direct corrections). We will use the definitions [52, 53]

$$\begin{aligned} S &= -16\pi \frac{\Pi_{3Y}(M_Z^2) - \Pi_{3Y}(0)}{M_Z^2}, \\ T &= \frac{4\pi}{M_Z^2 s_W^2 c_W^2} [\Pi_{11}(0) - \Pi_{33}(0)], \\ U &= 16\pi \left( \frac{\Pi_{11}(M_W^2) - \Pi_{11}(0)}{M_W^2} - \frac{\Pi_{33}(M_Z^2) - \Pi_{33}(0)}{M_Z^2} \right). \end{aligned} \quad (19)$$

They are equivalent to the ones used in Ref. [5], as can be seen by a change of basis. In these expressions only the contributions of new particles are meant to be included. Radiative corrections from SM particles must be treated separately because their leading effects are direct, not oblique. The parameters  $S$ ,  $T$ ,  $U$  are extracted from precision electroweak observables, and their most recent values are in Table 4. The contributions to  $S$ ,  $T$  and  $U$  of an arbitrary number of families plus vector-like singlets and doublets have been computed in Ref. [53]. In our models there are no exotic vector-like doublets, hence right-handed currents are absent and their expressions simplify to

$$\begin{aligned} S &= \frac{N_c}{2\pi} \left( \sum_{\alpha=1}^{\mathcal{N}_u} \sum_{\sigma=1}^{\mathcal{N}_d} |V_{\alpha\sigma}|^2 \psi_+(y_\alpha, y_\sigma) - \sum_{\beta < \alpha}^{\mathcal{N}_u} |X_{\alpha\beta}^u|^2 \psi_+(y_\alpha, y_\beta) - \sum_{\tau < \sigma}^{\mathcal{N}_d} |X_{\sigma\tau}^d|^2 \psi_+(y_\sigma, y_\tau) \right), \\ T &= \frac{N_c}{16\pi s_W^2 c_W^2} \left( \sum_{\alpha=1}^{\mathcal{N}_u} \sum_{\sigma=1}^{\mathcal{N}_d} |V_{\alpha\sigma}|^2 \theta_+(y_\alpha, y_\sigma) - \sum_{\beta < \alpha}^{\mathcal{N}_u} |X_{\alpha\beta}^u|^2 \theta_+(y_\alpha, y_\beta) - \sum_{\tau < \sigma}^{\mathcal{N}_d} |X_{\sigma\tau}^d|^2 \theta_+(y_\sigma, y_\tau) \right), \\ U &= -\frac{N_c}{2\pi} \left( \sum_{\alpha=1}^{\mathcal{N}_u} \sum_{\sigma=1}^{\mathcal{N}_d} |V_{\alpha\sigma}|^2 \chi_+(y_\alpha, y_\sigma) - \sum_{\beta < \alpha}^{\mathcal{N}_u} |X_{\alpha\beta}^u|^2 \chi_+(y_\alpha, y_\beta) - \sum_{\tau < \sigma}^{\mathcal{N}_d} |X_{\sigma\tau}^d|^2 \chi_+(y_\sigma, y_\tau) \right), \end{aligned} \quad (20)$$

where  $N_c = 3$  is the number of colours,  $y_i = (m_i/M_Z)^2$  and we use the  $\overline{\text{MS}}$  definition of  $s_W^2$ , as well as  $\overline{\text{MS}}$  masses at the scale  $M_Z$ . The functions multiplying the mixing angles are

$$\begin{aligned}
\psi_+(y_1, y_2) &= \frac{22y_1 + 14y_2}{9} - \frac{1}{9} \log \frac{y_1}{y_2} + \frac{11y_1 + 1}{18} f(y_1, y_1) + \frac{7y_2 - 1}{18} f(y_2, y_2), \\
\theta_+(y_1, y_2) &= y_1 + y_2 - \frac{2y_1y_2}{y_1 - y_2} \log \frac{y_1}{y_2}, \\
\chi_+(y_1, y_2) &= \frac{y_1 + y_2}{2} - \frac{(y_1 - y_2)^2}{3} + \left[ \frac{(y_1 - y_2)^3}{6} - \frac{y_1^2 + y_2^2}{2(y_1 - y_2)} \right] \log \frac{y_1}{y_2} \\
&\quad + \frac{y_1 - 1}{6} f(y_1, y_1) + \frac{y_2 - 1}{6} f(y_2, y_2) \\
&\quad + \left[ \frac{1}{3} - \frac{y_1 + y_2}{6} - \frac{(y_1 - y_2)^2}{6} \right] f(y_1, y_2). \tag{21}
\end{aligned}$$

The function  $f$  is defined as

$$f(y_1, y_2) = \begin{cases} -2\sqrt{\Delta} \left( \arctan \frac{y_1 - y_2 + 1}{\sqrt{\Delta}} - \arctan \frac{y_1 - y_2 - 1}{\sqrt{\Delta}} \right) & \Delta > 0 \\ \sqrt{-\Delta} \log \frac{y_1 + y_2 - 1 + \sqrt{-\Delta}}{y_1 + y_2 - 1 - \sqrt{-\Delta}} & \Delta \leq 0 \end{cases}, \tag{22}$$

with  $\Delta = -1 - y_1^2 - y_2^2 + 2y_1 + 2y_2 + 2y_1y_2$ . The functions  $\psi$ ,  $\theta$ ,  $\chi$  are symmetric under the interchange of their variables, and  $\theta$ ,  $\chi$  satisfy  $\theta(y, y) = 0$ ,  $\chi(y, y) = 0$ .

$S$	$-0.03 \pm 0.11$
$T$	$-0.02 \pm 0.13$
$U$	$0.24 \pm 0.13$

Table 4: Experimental values of the oblique parameters.

These expressions are far from transparent, and to have a better understanding of them we will examine the example of an up singlet mixing exclusively with the top. In this limit, the new contributions are

$$\begin{aligned}
S &= \frac{N_c}{2\pi} \left\{ |V_{Tb}|^2 [\psi_+(y_T, y_b) - \psi_+(y_t, y_b)] - |X_{Tt}|^2 \psi_+(y_T, y_t) \right\}, \\
T &= \frac{N_c}{16\pi s_W^2 c_W^2} \left\{ |V_{Tb}|^2 [\theta_+(y_T, y_b) - \theta_+(y_t, y_b)] - |X_{Tt}|^2 \theta_+(y_T, y_t) \right\}, \\
U &= -\frac{N_c}{2\pi} \left\{ |V_{Tb}|^2 [\chi_+(y_T, y_b) - \chi_+(y_t, y_b)] - |X_{Tt}|^2 \chi_+(y_T, y_t) \right\}. \tag{23}
\end{aligned}$$

The factors  $|V_{Tb}|^2$ ,  $|X_{Tt}|^2$  describing the mixing of the quark  $T$  are not independent: as can be seen from the results in Section 2, for  $n_u = 1$  we have the relation

$$|X_{Tt}|^2 = |V_{Tb}V_{tb}|^2 = |V_{Tb}|^2(1 - |V_{Tb}|^2). \quad (24)$$

For  $t$  and  $T$  degenerate,  $T$  and  $U$  would automatically vanish independently of the mixing, and  $S = -0.16 |X_{Tt}|^2$ . In order to obtain a simple approximate formula when  $m_T \gg m_t$ , we approximate  $1 - |V_{Tb}|^2 \sim 1$  and keep only the leading order in  $y_T$ . (Needless to say, we use Eqs. (20–22) for our fits.) Using the numerical values of  $y_b$ ,  $y_t$ , this yields

$$\begin{aligned} S &= \frac{N_c}{2\pi} |V_{Tb}|^2 \left[ -0.34 + O(y_T^{-1}) \right], \\ T &= \frac{N_c}{16\pi s_W^2 c_W^2} |V_{Tb}|^2 \left[ -18.4 + 7.8 \log y_T + O(y_T^{-1}) \right], \\ U &= -\frac{N_c}{2\pi} |V_{Tb}|^2 \left[ -0.60 + O(y_T^{-1}) \right]. \end{aligned} \quad (25)$$

These expressions give a fair estimate of the effect of the top mixing in the oblique parameters. We notice that the effect on  $S$ ,  $U$  is very small,  $S = -0.16 |V_{Tb}|^2$ ,  $U = 0.29 |V_{Tb}|^2$ , but sizeable for  $T$  (for instance,  $T = 2.7 |V_{Tb}|^2$  for  $\overline{m}_T = 500$  GeV). Indeed, the  $T$  parameter bounds the CKM matrix element  $V_{Tb}$  (and hence  $V_{tb}$ ) more effectively than the radiative correction to  $R_b$  and better than low energy observables.

In Model II the analysis is similar, but the constraints from  $R_b$  and FCN processes at low energies are much more restrictive than these from oblique corrections.

## 5 Limits from FCN processes at low energies

In this Section we discuss low energy processes involving meson mixing and/or decays. An important point is that almost all the observables analysed receive short-distance contributions from box and/or penguin diagrams with  $Q = 2/3$  quark loops (otherwise it will be indicated explicitly). The top amplitudes are specially relevant due to the large top mass, and are proportional to  $V_{td}^*V_{ts}$ ,  $V_{td}^*V_{tb}$  or  $V_{ts}^*V_{tb}$  (or their squares), depending on the meson considered. The observables are then sensitive to  $V_{td}$  and  $V_{ts}$ . (Also to  $V_{tb}$ , but the most important restrictions on its modulus come from precision measurements examined in last Section.) Additionally, there are extra contributions in the models under study: either new box and penguin diagrams with an internal  $T$  quark in Model I or diagrams with tree-level flavour-changing neutral currents (FCNC)

mediated by the  $Z$  boson in Model II. In any case, the new terms depend on products of two elements of the fourth row of  $V$  ( $V_{Td}^*V_{Ts}$ ,  $V_{Td}^*V_{Tb}$  or  $V_{Ts}^*V_{Tb}$  in Model I and FCN couplings  $X_{ds}$ ,  $X_{db}$  or  $X_{sb}$  in Model II).

The *a priori* unknown top and new physics terms are added coherently in the expressions of all these observables. Then, in principle there may exist a “conspiracy” between top and new physics contributions, with the first very different from the SM prediction and new physics making up for the difference. As long as we use a sufficiently exhaustive set of low energy observables and reproduce their experimental values, this possibility can be limited. This is because the products  $V_{td}^*V_{ts}$ ,  $\dots$ ,  $V_{Td}^*V_{Ts}$  or  $X_{ds}$ , etc. appear in the expressions of these observables in combinations with different coefficients.

Our observables for Models I and II include  $|\delta m_B|$ ,  $|\delta m_{B_s}|$ ,  $\varepsilon$ ,  $\varepsilon'/\varepsilon$ , the branching ratios for  $b \rightarrow se^+e^-$ ,  $b \rightarrow s\mu^+\mu^-$ ,  $K^+ \rightarrow \pi^+\nu\bar{\nu}$ ,  $K_L \rightarrow \mu^+\mu^-$  and the CP asymmetry  $a_{\psi K_S}$ . For model I we use  $|\delta m_D|$  as well. It must be stressed that *they are all independent* and give additional information that cannot be obtained from the rest. For example, if we remove  $\varepsilon$  from the list we can find choices of parameters of our models for which all the remaining observables agree with experiment (the precise criteria of agreement used will be specified in Section 8) but  $\varepsilon$  is more than 5 standard deviations from its measured value. This procedure applied to each one shows that none of them can be dismissed.

Once the values of the observables in these sets are in agreement with experiment, the predictions for the mass difference  $|\delta m_K|$  and some other partial rates, like  $b \rightarrow s\gamma$ ,  $B \rightarrow s\nu\bar{\nu}$ ,  $B \rightarrow \mu^+\mu^-$ ,  $B_s \rightarrow \mu^+\mu^-$ , agree with SM expectations ( $b \rightarrow s\gamma$  is nevertheless included in the fits). An important exception is the decay  $K_L \rightarrow \pi^0\nu\bar{\nu}$ , which will be studied in Section 7. Several CP asymmetries can also differ from SM expectations, and are thus good places to search for departures from the SM or further restrict the models under consideration.

In the rest of this Section we review the theoretical calculation within Models I and II of the observables listed above, together with their experimental status.

## 5.1 Neutral meson oscillations

### 5.1.1 The $\Delta F = 2$ effective Lagrangians

The complete Lagrangian for  $Q = -1/3$  external quarks in the presence of extra down singlets has been obtained in Ref. [54] and we follow their discussion except for small changes in the notation. We ignore QCD corrections for the moment and neglect external masses. The Lagrangians for  $K^0$ ,  $B^0$  and  $B_s^0$  oscillations are similar up to CKM factors, and for simplicity in the notation we refer to the kaon system. The box contributions can be written as

$$\mathcal{L}_{\text{eff}}^{\text{box}} = -\frac{G_F}{\sqrt{2}} \frac{\alpha}{4\pi s_W^2} \left[ \sum_{\alpha,\beta=u,c,t} \lambda_{sd}^\alpha \lambda_{sd}^\beta F(x_\alpha, x_\beta) \right] (\bar{s}_L \gamma^\mu d_L) (\bar{s}_L \gamma_\mu d_L), \quad (26)$$

with  $\lambda_{sd}^\alpha = V_{\alpha s}^* V_{\alpha d}$ , etc. The function  $F$  is not gauge-invariant, and its expression in the 't Hooft-Feynman gauge can be found *e. g.* in Ref. [55]. (This and other Inami-Lim [56] functions are collected in Appendix B.) The terms involving the  $u$  quark can be eliminated using

$$\sum_\alpha \lambda_{sd}^\alpha = X_{sd} \quad (27)$$

and setting  $x_u = 0$ , resulting in

$$\begin{aligned} \mathcal{L}_{\text{eff}}^{\text{box}} = & -\frac{G_F}{\sqrt{2}} \frac{\alpha}{4\pi s_W^2} \left[ \sum_{\alpha,\beta=c,t} \lambda_{sd}^\alpha \lambda_{sd}^\beta S_0(x_\alpha, x_\beta) + 8 X_{sd} \sum_{\alpha=c,t} \lambda_{sd}^\alpha B_0(x_\alpha) + X_{sd}^2 \right] \\ & \times (\bar{s}_L \gamma^\mu d_L) (\bar{s}_L \gamma_\mu d_L), \end{aligned} \quad (28)$$

where the gauge-independent function  $S_0$  is given in terms of the true box function  $F$  by

$$S_0(x_\alpha, x_\beta) = F(x_\alpha, x_\beta) - F(x_\alpha, 0) - F(0, x_\beta) + F(0, 0), \quad (29)$$

and  $B_0$  is given in terms of  $F$  by

$$4 B_0(x_\alpha) = F(x_\alpha, 0) - F(0, 0). \quad (30)$$

In addition there are two terms to be included in the Lagrangian. The first corresponds to  $Z$  tree-level FCNC,

$$\mathcal{L}_{\text{eff}}^Z = -\frac{G_F}{\sqrt{2}} X_{sd}^2 (\bar{s}_L \gamma^\mu d_L) (\bar{s}_L \gamma_\mu d_L). \quad (31)$$

The second is originated from diagrams with one tree-level FCN coupling and one triangle loop. Its contribution plus the  $B_0$  term in Eq. (28) can be compared with the short-distance effective Lagrangian for  $K^0 \rightarrow \mu^+ \mu^-$  (see Ref. [54] for the details), concluding that the sum of both gives the gauge-invariant Inami-Lim function  $Y_0$  with a minus sign. The full gauge-invariant  $\Delta S = 2$  effective Lagrangian then reads

$$\begin{aligned} \mathcal{L}_{\text{eff}}^{\text{II}} &= -\frac{G_F}{\sqrt{2}} \left[ \frac{\alpha}{4\pi s_W^2} \sum_{\alpha,\beta=c,t} \lambda_{sd}^\alpha \lambda_{sd}^\beta S_0(x_\alpha, x_\beta) - 8 \frac{\alpha}{4\pi s_W^2} X_{sd} \sum_{\alpha=c,t} \lambda_{sd}^\alpha Y_0(x_\alpha) + X_{sd}^2 \right] \\ &\times (\bar{s}_L \gamma^\mu d_L) (\bar{s}_L \gamma_\mu d_L) . \end{aligned} \quad (32)$$

We use the II superscript to refer to model II. The  $X_{ds}^2$  term in Eq. (26) is subleading with respect to  $\mathcal{L}_{\text{eff}}^Z$ , and it has been omitted.

The SM Lagrangian can be readily recovered setting  $X_{ds} = 0$  in the above equation. In Model I the Lagrangian reduces to the SM-like box contributions but with terms involving the new mass eigenstate  $T$ ,

$$\mathcal{L}_{\text{eff}}^{\text{I}} = -\frac{G_F}{\sqrt{2}} \left[ \frac{\alpha}{4\pi s_W^2} \sum_{\alpha,\beta=c,t,T} \lambda_{sd}^\alpha \lambda_{sd}^\beta S_0(x_\alpha, x_\beta) \right] (\bar{s}_L \gamma^\mu d_L) (\bar{s}_L \gamma_\mu d_L) . \quad (33)$$

In the  $B^0$  and  $B_s^0$  systems the approximation of vanishing external masses is not justified for the  $b$  quark. However, the two terms involving  $S_0(x_c) \equiv S_0(x_c, x_c)$  and  $S_0(x_c, x_t)$  are much smaller than the one with  $S_0(x_t) \equiv S_0(x_t, x_t)$  and can be neglected, and for the latter  $m_b \ll m_t$  and the approximation is valid. The effective Lagrangian for  $D^0 - \bar{D}^0$  mixing is more problematic and we will deal with it later.

Short-distance QCD corrections are included in these Lagrangians as  $\eta$  factors multiplying each term in the usual way. These factors account for high energy QCD effects and renormalisation group (RG) evolution to lower scales [57]. When available, we use next-to-leading order (NLO) corrections [58]. For the nonstandard contributions we use leading logarithmic (LL) RG evolution [59]. The differences between LL and NLO corrections are minimal provided we use  $\overline{\text{MS}}$  masses  $\overline{m}_i(m_i)$  in the evaluations [58]. Some representative QCD corrections for the new terms are

$$\begin{aligned} \eta_Z^K &= [\alpha_s(m_c)]^{\frac{6}{27}} \left[ \frac{\alpha_s(m_b)}{\alpha_s(m_c)} \right]^{\frac{6}{25}} \left[ \frac{\alpha_s(M_Z)}{\alpha_s(m_b)} \right]^{\frac{6}{23}} , \\ \eta_{TT}^B &= [\alpha_s(m_t)]^{\frac{6}{23}} \left[ \frac{\alpha_s(m_T)}{\alpha_s(m_t)} \right]^{\frac{6}{21}} . \end{aligned} \quad (34)$$

Here the superscripts  $K, B$  refer to the neutral mesons, and the subscripts to the term considered.



### 5.1.2 $K^0$ oscillations

The element  $M_{12}$  of the  $K^0 - \bar{K}^0$  mixing matrix is obtained from the effective Lagrangian (see for instance Ref. [57]),

$$M_{12}^K = \frac{G_F^2 M_W^2 f_K^2 \hat{B}_K m_{K^0}}{12\pi^2} \left[ (\lambda_{ds}^c)^2 \eta_{cc}^K S_0(x_c) + (\lambda_{ds}^t)^2 \eta_{tt}^K S_0(x_t) + 2\lambda_{ds}^c \lambda_{ds}^t \eta_{ct}^K S_0(x_c, x_t) + \Delta_K \right]. \quad (35)$$

In this expression  $m_{K^0} = 498$  MeV is the  $K^0$  mass,  $f_K = 160$  MeV the kaon decay constant taken from experiment and  $\hat{B}_K = 0.86 \pm 0.15$  [60] is the bag parameter. The QCD corrections are  $\eta_{cc}^K = 1.38 \pm 0.20$ ,  $\eta_{tt}^K = 0.57$ ,  $\eta_{ct}^K = 0.47$  [61] (we do not explicitly write the errors when they are negligible). The extra piece  $\Delta_K$  in models I and II is

$$\begin{aligned} \Delta_K^{\text{I}} &= (\lambda_{ds}^T)^2 \eta_{TT}^K S_0(x_T) + 2\lambda_{ds}^c \lambda_{ds}^T \eta_{cT}^K S_0(x_c, x_T) + 2\lambda_{ds}^t \lambda_{ds}^T \eta_{tT}^K S_0(x_t, x_T), \\ \Delta_K^{\text{II}} &= -8X_{ds} \left[ \lambda_{ds}^c \eta_Z^K Y_0(x_c) + \lambda_{ds}^t \eta_{tt}^K Y_0(x_t) \right] + \frac{4\pi s_W^2}{\alpha} \eta_Z^K X_{ds}^2, \end{aligned} \quad (36)$$

with  $\eta_{TT}^K = 0.58$ ,  $\eta_Z^K = 0.60$ . We estimate  $\eta_{cT}^K \simeq \eta_{ct}^K$ ,  $\eta_{tT}^K \simeq \eta_{TT}^K$ , and expect that this is a good approximation because RG evolution is slower at larger scales.

In the neutral kaon system the mass difference  $\delta m_K$  can be written as

$$\delta m_K = 2 \text{Re } M_{12}^K + \delta m_K^{\text{LD}} \quad (37)$$

where the second term is a long-distance contribution that cannot be calculated reliably. For the first term we obtain  $(4.64 \pm 0.68) \times 10^{-3} \text{ ps}^{-1}$  within the SM, whereas  $\delta m_K = 5.30 \times 10^{-3} \text{ ps}^{-1}$ . The large  $\sim 30\%$  long-distance contribution prevents us from using  $\delta m_K$  as a constraint on our models, but we observe anyway that the short-distance part  $2 \text{Re } M_{12}^K$  always takes values very close to the SM prediction once all other constraints are fulfilled.

The CP violating parameter  $\varepsilon$  is calculated as <sup>3</sup>

$$\varepsilon = e^{i\pi/4} \frac{\text{Im } M_{12}^K}{\sqrt{2} \delta m_K} \quad (38)$$

and in the SM it is close to its experimental value  $(2.282 \pm 0.017) \times 10^{-3}$  after a proper choice of the CKM phase  $\delta$  (see Appendix A). The SM prediction with the

<sup>3</sup>This expression assumes a phase convention where  $V_{ud}^* V_{us}$  is real. For a rephasing-invariant definition of  $\varepsilon$  see Ref. [62].

phase  $\delta = 1.014$  that best fits  $\varepsilon$ ,  $\varepsilon'/\varepsilon$ ,  $a_{\psi K_S}$  and  $|\delta m_B|$  is  $\varepsilon = (2.18 \pm 0.38) \times 10^{-3}$ . Notice that there is a large theoretical error in the calculation, mainly a consequence of the uncertainty in  $\hat{B}_K$ , which results in a poor knowledge of the CKM phase that reproduces  $\varepsilon$  within the SM. In Models I and II this parameter receives contributions from several CP violating phases and thus it cannot be used to extract one in particular. Instead, we let the phases arbitrary and require that the prediction for  $\varepsilon$  agrees with experiment.

### 5.1.3 $B^0$ oscillations

The element  $M_{12}^B$  of the  $B^0 - \bar{B}^0$  mixing matrix is

$$M_{12}^B = \frac{G_F^2 M_W^2 f_B^2 \hat{B}_B m_{B^0}}{12\pi^2} [(\lambda_{db}^t)^2 \eta_{tt}^B S_0(x_t) + \Delta_B] \quad (39)$$

with  $m_{B^0} = 5.279$  GeV. We use  $f_B = 200 \pm 30$  MeV,  $\hat{B}_B = 1.30 \pm 0.18$  from lattice calculations [63]. The terms corresponding to  $S_0(x_c)$  and  $S_0(x_c, x_t)$  have been discarded as usual, because in the SM, as well as in our models, they are numerically 2–3 orders of magnitude smaller than the  $S_0(x_t)$  term (the CKM angles are of the same order and the  $S_0$  functions are much smaller). The QCD correction is  $\eta_{tt}^B = 0.55$ . The nonstandard contributions are

$$\begin{aligned} \Delta_B^{\text{I}} &= (\lambda_{db}^T)^2 \eta_{TT}^B S_0(x_T) + 2\lambda_{db}^t \lambda_{db}^T \eta_{tT}^B S_0(x_t, x_T), \\ \Delta_B^{\text{II}} &= -8X_{db} \lambda_{db}^t \eta_{tt}^B Y_0(x_t) + \frac{4\pi s_W^2}{\alpha} \eta_Z^B X_{db}^2. \end{aligned} \quad (40)$$

The terms  $S_0(x_c, x_T)$  in  $\Delta_B^{\text{I}}$  and  $Y_0(x_c)$  in  $\Delta_B^{\text{II}}$  have been dropped with the same argument as above. The QCD corrections for the rest are  $\eta_{TT}^B = 0.55$ ,  $\eta_Z^B = 0.57$  and we approximate  $\eta_{tT}^B \simeq \eta_{TT}^B$ .

Since  $|\Gamma_{12}^B| \ll |M_{12}^B|$ , the mass difference in the  $B$  system is

$$|\delta m_B| = 2|M_{12}^B|, \quad (41)$$

and is useful to constrain  $\lambda_{db}^t$  and the new physics parameters,  $\lambda_{db}^T$  or  $X_{db}$  depending on the model considered. Long-distance effects are negligible in the  $B$  system, and the SM calculation yields  $|\delta m_B| = 0.49 \pm 0.16$  ps<sup>-1</sup>, to be compared with the experimental value  $0.489 \pm 0.008$  ps<sup>-1</sup>.

A second restriction regarding  $B$  oscillations comes from the time-dependent asymmetry in the decay  $B^0 \rightarrow \psi K_S$  (see for instance Ref. [62] for a precise definition). This

process is mediated by the quark-level transition  $\bar{b} \rightarrow \bar{c}c\bar{s}$  and takes place at tree-level, with small penguin corrections. The amplitude for the decay can then be written to a good approximation as  $A = \tilde{A} V_{cb}^* V_{cs}$ , with  $\tilde{A}$  real. Therefore the asymmetry is [8]  $a_{\psi K_S} = \text{Im } \lambda_{\psi K_S}$ , with

$$\lambda_{\psi K_S} = -\frac{(M_{12}^B)^*}{|M_{12}^B|} \frac{\tilde{A}}{A} \frac{M_{12}^K}{|M_{12}^K|} = -\frac{(M_{12}^B)^*}{|M_{12}^B|} \frac{V_{cb} V_{cs}^*}{V_{cb}^* V_{cs}} \frac{M_{12}^K}{|M_{12}^K|} \quad (42)$$

and provides a constraint on the combination of phases of  $B$ ,  $K$  mixing and the decay  $\bar{b} \rightarrow \bar{c}c\bar{s}$ , which are functions of the CKM CP violating phases and angles. Our calculation within the SM gives  $a_{\psi K_S} = 0.71$ , and with other choices of parameters for the CKM matrix the prediction may change in  $\pm 0.08$ . The world average is  $a_{\psi K_S} = 0.734 \pm 0.054$  [64]. This asymmetry can also be expressed as

$$a_{\psi K_S} = \sin(2\beta + 2\theta_B - 2\theta_K), \quad (43)$$

with  $\beta$  one of the angles of the well-known  $db$  unitarity triangle,

$$\beta = \arg \left[ -\frac{V_{cd} V_{cb}^*}{V_{td} V_{tb}^*} \right], \quad (44)$$

and  $\theta_B, \theta_K$  parameterising the deviation of the mixing amplitude phases with respect to the SM,

$$2\theta_B = \arg \frac{M_{12}^B}{(M_{12}^B)_{\text{SM}}}, \quad 2\theta_K = \arg \frac{M_{12}^K}{(M_{12}^K)_{\text{SM}}}. \quad (45)$$

In the absence of new physics, or if the extra phases  $\theta_B, \theta_K$  cancel,  $a_{\psi K_S} = \sin 2\beta$ .

The phase of  $M_{12}^K$  is relatively fixed by the determination of  $\varepsilon$  and  $\delta m_K$ . Despite the good experimental precision of both measurements, the former has a large theoretical uncertainty from  $\hat{B}_K$  and the latter from long-distance contributions. This allows  $\theta_K$  to be different from zero, but it must be small anyway. The agreement of  $a_{\psi K_S}$  with experiment then constrains the phase  $\theta_B$ . The asymmetry in semileptonic decays depends also on  $\theta_B$  [65] and does not provide any extra constraint on the parameters of these models.

#### 5.1.4 $B_s^0$ oscillations

The analysis of  $B_s^0$  oscillations is very similar to the previous one for the  $B^0$  system, with

$$M_{12}^{B_s} = \frac{G_F^2 M_W^2 f_{B_s}^2 \hat{B}_{B_s} m_{B_s}^0}{12\pi^2} \left[ (\lambda_{sb}^t)^2 \eta_{tt}^{B_s} S_0(x_t) + \Delta_{B_s} \right] \quad (46)$$

and  $m_{B_s^0} = 5.370$  GeV,  $f_{B_s} = 230 \pm 35$  MeV,  $\hat{B}_{B_s} = 1.30 \pm 0.18$  [63]. The  $S_0(x_c)$  and  $S_0(x_c, x_t)$  terms have again been neglected, and the QCD correction for the  $S_0(x_t)$  term is  $\eta_{tt}^{B_s} = 0.55$ . The new contributions are

$$\begin{aligned}\Delta_{B_s}^{\text{I}} &= (\lambda_{sb}^T)^2 \eta_{TT}^{B_s} S_0(x_T) + 2\lambda_{sb}^t \lambda_{sb}^T \eta_{tT}^{B_s} S_0(x_t, x_T), \\ \Delta_{B_s}^{\text{II}} &= -8X_{sb} \lambda_{sb}^t \eta_{tt}^{B_s} Y_0(x_t) + \frac{4\pi s_W^2}{\alpha} \eta_Z^{B_s} X_{sb}^2.\end{aligned}\quad (47)$$

with the terms involving  $S_0(x_c, x_T)$  in  $\Delta_{B_s}^{\text{I}}$  and  $Y_0(x_c)$  in  $\Delta_{B_s}^{\text{II}}$  discarded. The QCD correction factors are the same as for  $M_{12}^B$ . The SM estimate for  $|\delta m_{B_s}| = 2|M_{12}^{B_s}|$  is  $17.6 \pm 5.9$  ps<sup>-1</sup>. Experimentally only a lower bound for  $|\delta m_{B_s}|$  exists,  $|\delta m_{B_s}| \geq 13.1$  ps<sup>-1</sup> with a 95% confidence level (CL), which can be saturated in Models I and II and thus provides a constraint not always considered in the literature. Larger values than in the SM are also possible.

### 5.1.5 $D^0$ oscillations

In contrast with the  $K^0$  and  $B^0$  systems,  $D^0$  mixing is mediated by box diagrams with  $Q = -1/3$  internal quarks. This circumstance leads to a very small mass difference in the SM, as a consequence of the GIM mechanism. In addition, the approximation of vanishing external masses is inconsistent, and with a careful analysis including the charm mass an extra suppression  $\sim (m_s/m_c)^2$  is found [66, 67], resulting in  $|\delta m_D| \sim 10^{-17}$  GeV. NLO contributions, for example dipenguin diagrams [68], are of the same order, but to our knowledge a full NLO calculation is not available yet. Long-distance contributions are estimated to be  $|\delta m_D| \sim 10^{-16}$  GeV [69].

On the other hand, the present experimental limit,  $|\delta m_D| < 0.07$  ps<sup>-1</sup> =  $4.6 \times 10^{-14}$  GeV with a 95 CL, is still orders of magnitude above SM expectations. This limit can be saturated in Model I with a tree-level FCN coupling  $X_{cu}$  [70]. In Model II with a new quark  $B$  the GIM suppression is partially removed but we have checked that  $D^0$  mixing does not provide any additional constraint for a mass  $m_B < 1$  TeV. Hence here we only discuss Model I. The element  $M_{12}^D$  is then

$$M_{12}^D = \frac{G_F^2 M_W^2 f_D^2 \hat{B}_D m_{D^0}}{12\pi^2} \left[ \frac{4\pi s_W^2}{\alpha} \eta_Z^D X_{cu}^2 \right], \quad (48)$$

where  $m_{D^0} = 1.865$  GeV and  $f_D = 215 \pm 15$  MeV [71]. We assume  $\hat{B}_D = 1.0 \pm 0.3$ . We have omitted the SM terms, whose explicit expression can be found for instance in Ref. [67], since they are generically much smaller than the one written above. In

contrast with  $K^0$  and  $B^0$  oscillations, the terms linear in  $X_{cu}$  are both negligible due to the small masses  $m_s$ ,  $m_b$ , and we have dropped them <sup>4</sup>. The QCD correction is  $\eta_Z^D = 0.59$ . The mass difference is given by  $|\delta m_D| = 2|M_{12}^D|$ , and provides the most stringent limit on  $X_{cu}$ .

## 5.2 $K$ decays

### 5.2.1 $K^+ \rightarrow \pi^+ \nu \bar{\nu}$

The importance of the rare kaon decay  $K^+ \rightarrow \pi^+ \nu \bar{\nu}$  in setting limits on the FCN coupling  $X_{sd}$  has been pointed out before [40]. This is a theoretically very clean process after NLO corrections reduce the scale dependence. The uncertainty in the hadronic matrix element can be avoided relating this process to the leading decay  $K^+ \rightarrow \pi^0 e^+ \bar{\nu}$  using isospin symmetry, and then using the measured rate for the latter:

$$\frac{\text{Br}(K^+ \rightarrow \pi^+ \nu \bar{\nu})}{\text{Br}(K^+ \rightarrow \pi^0 e^+ \bar{\nu})} = \frac{r_{K^+} \alpha^2}{2\pi^2 s_W^4 |V_{us}|^2} \sum_{l=e,\mu,\tau} \left| \lambda_{sd}^c X_{NL}^l + \lambda_{sd}^t \eta_t^X X_0(x_t) + \Delta_{K^+} \right|^2. \quad (49)$$

The factor  $r_{K^+} = 0.901$  [73] accounts for isospin breaking corrections. The charm contributions at NLO are [74]  $X_{NL}^{c;\mu} = (10.6 \pm 1.5) \times 10^{-4}$ ,  $X_{NL}^\tau = (7.1 \pm 1.4) \times 10^{-4}$ , and the QCD correction to the top term is  $\eta_t^X = 0.994$  [75]. The function  $X_0 = C_0 - 4B_0$  can be found in Appendix B. The top and charm terms have similar size because  $X_0(x_t) \gg X_{NL}^l$  but  $\lambda_{sd}^t \ll \lambda_{sd}^c$ . With  $\text{Br}(K^+ \rightarrow \pi^0 e^+ \bar{\nu}) = 0.0487$  we obtain the SM value  $\text{Br}(K^+ \rightarrow \pi^+ \nu \bar{\nu}) = (6.4 \pm 0.6) \times 10^{-11}$ , where in the uncertainty we only include that derived from  $m_t$  and  $X_{NL}^l$ , and not from CKM mixing angles. Experimentally there are only two  $K^+ \rightarrow \pi^+ \nu \bar{\nu}$  events [76]. The corresponding 90% CL interval for the branching ratio is  $[3.2, 48] \times 10^{-11}$ .

The new physics contributions are denoted by  $\Delta_{K^+}$ , and in Models I and II they read

$$\begin{aligned} \Delta_{K^+}^{\text{I}} &= \lambda_{sd}^T \eta_T^X X_0(x_T), \\ \Delta_{K^+}^{\text{II}} &= C_{U2Z} X_{sd}, \end{aligned} \quad (50)$$

where the factor  $C_{U2Z}$  in  $\Delta_{K^+}^{\text{II}}$  is [77]

$$C_{U2Z} = -\frac{\pi^2}{\sqrt{2} G_F M_W^2} = -\frac{\pi s_W^2}{\alpha}. \quad (51)$$

---

<sup>4</sup>Extending the discussion in Ref. [54] to the case of  $D^0 - \bar{D}^0$  mixing, we can argue that the functions multiplying the terms linear in  $X_{cu}$  are the Inami-Lim functions appearing in  $D^0 \rightarrow \mu^+ \mu^-$ , which are also in this case  $-Y_0$  [72].

In Model I there is another consequence of the mixing of the top quark not considered in these expressions:  $X_{tt}$  and  $X_{TT}$  are different from unity (hence the function  $C_0$  corresponding to  $Z$  penguins changes) and there are extra penguin diagrams with  $T$  and  $t$ , proportional to the FCN coupling  $X_{tT}$ . This is the same kind of modification that we have seen in the discussion of the radiative correction to  $R_b$ . There it was found that the net effect of the top mixing would cancel for  $m_T = m_t$  and is small for  $m_T \sim m_t$ . The magnitude of the correction required to take this effect into account in  $\text{Br}(K^+ \rightarrow \pi^+ \nu \bar{\nu})$  can be estimated in analogy with that case. We find that the correction grows with  $X_{tT}$  and  $m_T$ ; however, these cannot be both large, as required by oblique parameters. The result is that the error made using Eqs. (49,50) is smaller than the combined uncertainty from  $X_{NL}$  and  $m_t$  (10%). For  $X_{tT}$  in its upper limit it amounts to a 6% extra systematic error, unimportant with present experimental precision. For each value of  $X_{tT}$  and  $m_T$  we include the estimate of the correction required in the total theoretical uncertainty. Bearing in mind the approximation done in using Eqs. (49,50), we also omit the QCD factors in the calculation because they represent a smaller effect.

This decay sets relevant constraints on  $\lambda_{sd}^t$ ,  $\lambda_{sd}^T$  and  $X_{sd}$  that cannot be obtained from the rest of processes studied in this Section. This fact has been explicitly proved studying what the range of predictions for  $\text{Br}(K^+ \rightarrow \pi^+ \nu \bar{\nu})$  would be if the rest of the restrictions were fulfilled but not the one regarding  $K^+ \rightarrow \pi^+ \nu \bar{\nu}$ . Since in some regions of the parameter space  $\text{Br}(K^+ \rightarrow \pi^+ \nu \bar{\nu})$  would be out of the experimental interval, this process cannot be discarded in the analysis.

### 5.2.2 $K_L \rightarrow \mu^+ \mu^-$

A complementary limit on  $\lambda_{sd}^t$ ,  $\lambda_{sd}^T$  and  $X_{sd}$  comes from the short-distance contribution to the decay  $K_L \rightarrow \mu^+ \mu^-$ . Although theoretically this is a clean calculation, the extraction from actual experimental data is very difficult. The branching ratio  $\text{Br}(K_L \rightarrow \mu^+ \mu^-) = 7.18 \pm 0.17 \times 10^{-9}$  [78], can be decomposed in a dispersive part  $[\text{Re } A]^2$  and an absorptive part  $[\text{Im } A]^2$ . The imaginary part can be calculated from  $\text{Br}(K_L \rightarrow \gamma \gamma)$  and amounts to  $(7.07 \pm 0.18) \times 10^{-9}$  [5], which almost saturates the total rate. The extraction of the long-distance component from the real part  $[\text{Re } A]^2 = (1.1 \pm 2.4) \times 10^{-10}$  is not model-independent [79], but as long as our aim is to place limits on new physics we can use the model in Ref. [80] as an estimate, obtaining the 90% CL bound  $\text{Re } A_{\text{SD}} \leq 1.9 \times 10^{-9}$ .

On the theoretical side, the calculation of the short-distance part of the decay is done relating it to  $K^+ \rightarrow \mu^+\nu$ ,

$$\frac{\text{Br}(K_L \rightarrow \mu^+\mu^-)_{\text{SD}}}{\text{Br}(K^+ \rightarrow \mu^+\nu)} = \frac{\tau_{K_L}}{\tau_{K^+}} \frac{\alpha^2}{\pi^2 s_W^4 |V_{us}|^2} \times \left[ Y_{NL} \text{Re} \lambda_{sd}^c + \eta_t^Y Y_0(x_t) \text{Re} \lambda_{sd}^t + \Delta_{K_L} \right]^2, \quad (52)$$

with  $\tau_{K_L} = 5.17 \times 10^{-8}$  s,  $\tau_{K^+} = 1.238 \times 10^{-8}$  s. The factor in the charm term is  $Y_{NL} = (2.94 \pm 0.28) \times 10^{-4}$  at NLO [74]. The function  $Y_0 = C_0 - B_0$  can be found in Appendix B, and the QCD correction for the top is very close to unity,  $\eta_t^Y = 1.012$  [75]. Using  $\text{Br}(K^+ \rightarrow \mu^+\nu) = 0.6343$  from experiment, the SM prediction is  $\text{Br}(K_L \rightarrow \mu^+\mu^-)_{\text{SD}} = (6.6 \pm 0.6) \times 10^{-10}$ . The new physics contributions are

$$\begin{aligned} \Delta_{K_L}^{\text{I}} &= \eta_T^Y Y_0(x_T) \text{Re} \lambda_{sd}^T, \\ \Delta_{K_L}^{\text{II}} &= \text{Re} C_{U2Z} X_{sd}. \end{aligned} \quad (53)$$

As in  $K^+ \rightarrow \pi^+\nu\bar{\nu}$  the mixing of the top quark modifies the Inami-Lim function  $C_0$  and adds a new  $t-T$  term. The net effect is small and has been taken into account in the theoretical uncertainty.

## 5.3 B decays

### 5.3.1 $B \rightarrow X_s \gamma$

The inclusive decay width  $\Gamma(B \rightarrow X_s \gamma)$  can be well approximated by the parton-level width  $\Gamma(b \rightarrow s \gamma)$ . In order to reduce uncertainties, it is customary to calculate instead the ratio

$$R_\gamma \equiv \frac{\Gamma(b \rightarrow s \gamma)}{\Gamma(b \rightarrow ce\bar{\nu})} \quad (54)$$

and derive  $\Gamma(b \rightarrow s \gamma)$  from  $R_\gamma$  and the experimental measurement of  $\Gamma(b \rightarrow ce\bar{\nu})$ . The ratio  $R_\gamma$  is given by

$$R_\gamma = \frac{|\lambda_{sb}^t|^2}{|V_{cb}|^2} \frac{6\alpha}{\pi f(z)} |C_{7\gamma}(\mu)|^2, \quad (55)$$

where  $z = m_c/m_b$  (pole masses) and

$$f(z) = 1 - 8z^2 + 8z^6 - z^8 - 24z^4 \log z \quad (56)$$

is a phase space factor for  $b \rightarrow ce\bar{\nu}$ . The Wilson coefficient  $C_{7\gamma}(\mu)$  is obtained from the relevant coefficients at the scale  $M_W$  by RG evolution.

The study of  $b \rightarrow s\gamma$  in the context of SM extensions with up and down quark singlets has been carried out at leading order (one loop) in Refs. [81, 82]. The Wilson coefficients at the scale  $M_W$  relevant for this process are, using the notation of Ref. [57],

$$\begin{aligned}
C_2(M_W) &= -\frac{\lambda_{sb}^c}{\lambda_{sb}^t}, \\
C_{7\gamma}(M_W) &= -\frac{1}{2}D'_0(x_t) + \Delta C_{7\gamma}(M_W), \\
C_{8G}(M_W) &= -\frac{1}{2}E'_0(x_t) + \Delta C_{8G}(M_W), \\
C_3(M_W) &= \Delta C_3(M_W), \\
C_7(M_W) &= \Delta C_7(M_W), \\
C_9(M_W) &= \Delta C_9(M_W).
\end{aligned} \tag{57}$$

The extra terms in Model I are straightforward to include,

$$\begin{aligned}
\Delta C_{7\gamma}^I(M_W) &= -\frac{1}{2}\frac{\lambda_{sb}^T}{\lambda_{sb}^t}D'_0(x_T), \\
\Delta C_{8G}^I(M_W) &= -\frac{1}{2}\frac{\lambda_{sb}^T}{\lambda_{sb}^t}E'_0(x_T), \\
\Delta C_3^I(M_W) &= 0, \\
\Delta C_7^I(M_W) &= 0, \\
\Delta C_9^I(M_W) &= 0.
\end{aligned} \tag{58}$$

In Model II there are contributions from  $Z$  penguins with one or two FCN couplings, plus  $H$  penguins and other terms originated by the non-unitarity of  $V$ . The expressions read [81]

$$\begin{aligned}
\Delta C_{7\gamma}^{\text{II}}(M_W) &= \frac{X_{sb}}{\lambda_{sb}^t} \left( \frac{23}{36} + \xi_s^Z + \xi_b^Z \right) + \frac{X_{sB} X_{Bb}}{\lambda_{sb}^t} [\xi_B^Z(y_B) + \xi_B^H(w_B)], \\
\Delta C_{8G}^{\text{II}}(M_W) &= \frac{X_{sb}}{\lambda_{sb}^t} \left( \frac{1}{3} - 3\xi_s^Z - 3\xi_b^Z \right) - 3\frac{X_{sB} X_{Bb}}{\lambda_{sb}^t} [\xi_B^Z(y_B) + \xi_B^H(w_B)], \\
\Delta C_3^{\text{II}}(M_W) &= -\frac{1}{6}\frac{X_{sb}}{\lambda_{sb}^t}, \\
\Delta C_7^{\text{II}}(M_W) &= -\frac{2}{3}s_W^2\frac{X_{sb}}{\lambda_{sb}^t}, \\
\Delta C_9^{\text{II}}(M_W) &= \frac{2}{3}(1 - s_W^2)\frac{X_{sb}}{\lambda_{sb}^t},
\end{aligned} \tag{59}$$

with  $y_i = (m_i/M_Z)^2$ ,  $w_i = (m_i/M_H)^2$ . The functions  $\xi$  are given in Appendix B. We have made the approximations  $y_s = 0$ ,  $y_b = 0$ ,  $m_s/m_b = 0$ , and a very small



term proportional to  $X_{sd}X_{db}$  has been omitted in  $\Delta C_{7\gamma}^{\text{II}}$  and  $\Delta C_{8G}^{\text{II}}$ . Note also that  $C_2(M_W) = 1$  in the SM, but not necessarily in Models I and II. The RG evolution to a scale  $\mu = 5$  GeV gives [81, 83]

$$\begin{aligned} C_{7\gamma}(\mu) = & -0.158 C_2(M_W) + 0.695 C_{7\gamma}(M_W) + 0.085 C_{8G}(M_W) \\ & + 0.143 C_3(M_W) + 0.101 C_7(M_W) - 0.036 C_9(M_W). \end{aligned} \quad (60)$$

From this coefficient we get  $R_\gamma = 2.62 \times 10^{-3}$  in the SM. In order to incorporate NLO corrections we normalise our LO calculation to the NLO value [84] with an *ad hoc* factor <sup>5</sup>  $K_\gamma = 1.12$ , and we keep the normalising factor for the calculation of  $R_\gamma$  in Models I and II. This is adequate provided the nonstandard contributions are small. The systematic error of this approximation is estimated to be smaller than  $\sim K_\gamma(K_\gamma - 1)[R_\gamma - R_\gamma(\text{SM})]$ , and vanishes if the new physics terms scale with the same factor  $K_\gamma$ . We have found that in practice this error is of order  $O(10^{-5})$ , and in the worst case  $2 \times 10^{-4}$ , smaller than the uncertainties present in the LO and NLO calculations. With this procedure and using  $\text{Br}(b \rightarrow ce\bar{\nu}) = 0.102$  we obtain  $\text{Br}(b \rightarrow s\gamma) = 3.34 \times 10^{-4}$ , in very good agreement with the world average  $(3.3 \pm 0.4) \times 10^{-4}$  [85, 86, 87]. We take as theoretical uncertainty the one quoted in Ref. [84],  $0.33 \times 10^{-4}$ .

### 5.3.2 $B \rightarrow X_s l^+ l^-$

The analysis of the decay  $B \rightarrow X_s l^+ l^-$  is very similar to the previous one of  $B \rightarrow X_s \gamma$ . Again, the process can be approximated by  $b \rightarrow sl^+ l^-$  and the quantity theoretically obtained is the differential ratio

$$R_{ll}(\hat{s}) \equiv \frac{1}{\Gamma(b \rightarrow ce\bar{\nu})} \frac{d}{d\hat{s}} \Gamma(b \rightarrow sl^+ l^-), \quad (61)$$

with  $\hat{s} = (p_{l^+} + p_{l^-})^2/m_b^2$  the normalised invariant mass of the lepton pair. The calculation at LO [88] involves two more operators at the scale  $M_W$ ,  $Q_{9V}$  and  $Q_{10A}$ . Defining for convenience  $\tilde{C}_{9V}$ ,  $\tilde{C}_{10A}$  by

$$C_{9V} = \frac{\alpha}{2\pi} \tilde{C}_{9V}, \quad C_{10A} = \frac{\alpha}{2\pi} \tilde{C}_{10A}, \quad (62)$$

the latter are

$$\begin{aligned} \tilde{C}_{9V}(M_W) &= -\frac{4}{9} \frac{\lambda_{sb}^c}{\lambda_{sb}^t} + \frac{Y_0(x_t)}{s_W^2} - 4Z_0(x_t) + \Delta\tilde{C}_{9V}(M_W), \\ \tilde{C}_{10A}(M_W) &= -\frac{Y_0(x_t)}{s_W^2} + \Delta\tilde{C}_{10A}(M_W). \end{aligned} \quad (63)$$

---

<sup>5</sup>We obtain the factor  $K_\gamma$  comparing our LO and the NLO calculation of  $R_\gamma$  in Ref. [84] with a common set of parameters.

The extra terms in Model I are analogous to the ones corresponding to the top,

$$\begin{aligned}\Delta\tilde{C}_{9V}^{\text{I}}(M_W) &= \frac{\lambda_{sb}^T}{\lambda_{sb}^t} \left[ \frac{Y_0(x_T)}{s_W^2} - 4Z_0(x_T) \right], \\ \Delta\tilde{C}_{10A}^{\text{I}}(M_W) &= -\frac{\lambda_{sb}^T}{\lambda_{sb}^t} \frac{Y_0(x_T)}{s_W^2},\end{aligned}\quad (64)$$

and in Model II we have [89]

$$\begin{aligned}\Delta\tilde{C}_{9V}^{\text{II}}(M_W) &= \left( \frac{1}{s_W^2} - 4 \right) C_{U2Z} \frac{X_{sb}}{\lambda_{sb}^t}, \\ \Delta\tilde{C}_{10A}^{\text{II}}(M_W) &= -\frac{C_{U2Z}}{s_W^2} \frac{X_{sb}}{\lambda_{sb}^t}.\end{aligned}\quad (65)$$

The RG evolution to a scale  $\mu = 5$  GeV gives the coefficients of the relevant operators,

$$\begin{aligned}C_1(\mu) &= -0.221 C_2(M_W), \\ C_2(\mu) &= 1.093 C_2(M_W), \\ \tilde{C}_{9V}(\mu) &= \tilde{C}_{9V}(M_W) + 1.838 C_2(M_W), \\ \tilde{C}_{10A}(\mu) &= \tilde{C}_{10A}(M_W),\end{aligned}\quad (66)$$

and  $C_{7\gamma}$  as in the process  $b \rightarrow s\gamma$ . We define for brevity in the notation an ‘‘effective’’  $\tilde{C}_{9V}$ ,

$$\tilde{C}_{9V}^{\text{eff}}(\mu) = \tilde{C}_{9V}(\mu) + g(z, \hat{s}) [3 C_1(\mu) + C_2(\mu)], \quad (67)$$

where the  $\hat{s}$ -dependent function  $g$  is [88]

$$\begin{aligned}g(z, \hat{s}) &= -\frac{8}{9} \log z + \frac{8}{27} + \frac{16}{9} \frac{z^2}{\hat{s}} \\ &\quad - \frac{2}{9} \sqrt{\left| 1 - \frac{4z^2}{\hat{s}} \right|} \left( 2 + \frac{4z^2}{\hat{s}} \right) \times \begin{cases} 2 \arctan \frac{1}{\sqrt{\frac{4z^2}{\hat{s}} - 1}} & \hat{s} < 4z^2 \\ \log \left| \frac{1 + \sqrt{1 - \frac{4z^2}{\hat{s}}}}{1 - \sqrt{1 - \frac{4z^2}{\hat{s}}}} \right| + \pi i & \hat{s} > 4z^2 \end{cases}.\end{aligned}\quad (68)$$

Then, the differential ratio  $R_{ll}$  is written as

$$\begin{aligned}R_{ll}(\hat{s}) &= \frac{\alpha^2}{4\pi^2 f(z)} \frac{|\lambda_{sb}^t|^2}{|V_{cb}|^2} (1 - \hat{s})^2 \left[ (1 + 2\hat{s}) (|\tilde{C}_{9V}^{\text{eff}}|^2 + |\tilde{C}_{10A}|^2) \right. \\ &\quad \left. + 4(1 + 2/\hat{s}) |\tilde{C}_{7\gamma}|^2 + 12 \text{Re} C_{7\gamma}^* \tilde{C}_{9V}^{\text{eff}} \right].\end{aligned}\quad (69)$$

The partial width  $\text{Br}(b \rightarrow sl^+l^-)$  is derived integrating  $\hat{s}$  from  $4m_l^2/m_b^2$  to one and multiplying by the experimental value of  $\text{Br}(b \rightarrow ce\bar{\nu})$ . Within the SM we obtain

$\text{Br}(b \rightarrow se^+e^-) = 7.3 \times 10^{-6}$ ,  $\text{Br}(b \rightarrow s\mu^+\mu^-) = 5.0 \times 10^{-6}$ . These values are a little sensitive to the precise value of  $s_W^2$  used. We use, as throughout the paper, the  $\overline{\text{MS}}$  definition. Experimentally,  $\text{Br}(b \rightarrow s\mu^+\mu^-) = (8.9 \pm 2.7) \times 10^{-6}$  but for electrons only an upper bound exists,  $\text{Br}(b \rightarrow se^+e^-) < 11.0 \times 10^{-6}$  with a 90% CL [90]. The NLO values [91] are 10% larger but in view of the experimental errors it is not necessary to incorporate NLO corrections to set limits on new physics. The theoretical uncertainties, including the possible modification of the  $C_0$  functions, do not have much importance either (in contrast with the decay  $b \rightarrow s\gamma$ ) and we do not take them into account in the statistical analysis.

Despite the worse experimental precision, in Model II  $b \rightarrow sl^+l^-$  sets a stronger limit on the FCN coupling  $X_{sb}$  than  $b \rightarrow s\gamma$ . This is understood because in this model the decay  $b \rightarrow sl^+l^-$  can be mediated by tree-level diagrams involving  $X_{sb}$ , while in the process  $b \rightarrow s\gamma$  this vertex appears only in extra penguin diagrams and unitarity corrections, of the same size as the SM contributions. Both  $l = e$  and  $l = \mu$  have to be considered, as the former sets the best upper bound and the latter provides a lower bound. In Model I it also gives a more restrictive constraint than  $b \rightarrow s\gamma$ , but we still include the latter in the fit.

## 5.4 The parameter $\varepsilon'$

This parameter measures direct CP violation in the kaon system (its definition can be found for instance in Ref. [62]). For several years the experimental measurements have been inconclusive, but now the determination has settled, with a present accuracy of  $\sim 10\%$ . On the contrary, the theoretical prediction is subject to large uncertainties. Instead of calculating  $\varepsilon'$  directly, we calculate  $\varepsilon'/\varepsilon \simeq \text{Re}\varepsilon'/\varepsilon$ , using the simplified expression [92]

$$\frac{\varepsilon'}{\varepsilon} = F_{\varepsilon'}(x_t) \text{Im} \lambda_{sd}^t + \Delta_{\varepsilon'} , \quad (70)$$

with

$$F_{\varepsilon'}(x_t) = P_0 + P_X X_0(x_t) + P_Y Y_0(x_t) + P_Z Z_0(x_t) + P_E E_0(x_t) \quad (71)$$

and  $\Delta_{\varepsilon'}$  representing the new physics contribution. The factors multiplying the Inami-Lim functions are

$$\begin{aligned} P_0 &= -3.167 + 12.409 B_6^{(1/2)} + 1.262 B_8^{(3/2)} , \\ P_X &= 0.540 + 0.023 B_6^{(1/2)} , \end{aligned}$$

$$\begin{aligned}
P_Y &= 0.387 + 0.088 B_6^{(1/2)}, \\
P_Z &= 0.474 - 0.017 B_6^{(1/2)} - 10.186 B_8^{(3/2)}, \\
P_E &= 0.188 - 1.399 B_6^{(1/2)} + 0.459 B_8^{(3/2)},
\end{aligned}
\tag{72}$$

with  $B_6^{(1/2)}$ ,  $B_8^{(3/2)}$  non-perturbative parameters specified below. The new contributions are

$$\begin{aligned}
\Delta_{\varepsilon'}^{\text{I}} &= F_{\varepsilon'}(x_T) \text{Im } \lambda_{sd}^T \\
\Delta_{\varepsilon'}^{\text{II}} &= C_{U2Z}(P_X + P_Y + P_Z) \text{Im } X_{sd}
\end{aligned}
\tag{73}$$

In  $\Delta_{\varepsilon'}^{\text{I}}$  we approximate the  $P$  coefficients in  $F_{\varepsilon'}(x_T)$  with the corresponding ones in  $F_{\varepsilon'}(x_t)$ . From lattice or large  $N_c$  calculations  $B_6^{(1/2)} = 1.0 \pm 0.3$ ,  $B_8^{(3/2)} = 0.8 \pm 0.2$ . Corrections accounting for final state interactions [93, 94] modify these figures to  $B_6^{(1/2)} = 1.55 \pm 0.5$ ,  $B_8^{(3/2)} = 0.7 \pm 0.2$  yielding  $\varepsilon'/\varepsilon = (1.64 \pm 0.70) \times 10^{-3}$  in good agreement with the world average  $(1.72 \pm 0.18) \times 10^{-3}$  [3, 4]. With large  $N_c$  expansions at NLO very similar results are obtained [95]. Notice that the large theoretical error in the  $B$  parameters partially takes into account the different values from different schemes. These uncertainties, together with cancellations among terms, bring about a large uncertainty in the prediction. In spite of this fact  $\varepsilon'/\varepsilon$  is very useful to constrain the imaginary parts of  $\lambda_{sd}^t$ ,  $\lambda_{sd}^T$  and  $X_{sd}$  [77].

## 5.5 Summary

The combined effect of the low energy constraints from  $K$  and  $B$  physics is to disallow large cancellations and “fine tuning” of parameters to some extent. As emphasised at the beginning of this Section, the various observables depend on the CKM angles  $V_{td}$ ,  $V_{ts}$ ,  $V_{tb}$  and the new physics parameters in different functional forms. Therefore, if theoretical and experimental precision were far better the parameter space would be constrained to a narrow window around the SM values, and perhaps other possible regions allowed by cancellations. However, as can be seen in Table 5, present theoretical and experimental precision allow for relatively large contributions of the new physics in Models I and II, with large deviations in some observables.

Other potential restrictions on these models have been explored: the rare decays  $B \rightarrow l^+l^-$ ,  $B_s \rightarrow l^+l^-$  and  $B \rightarrow X_s \nu \bar{\nu}$ . With present experimental precision they do not provide additional constraints, nor the predictions for their rates differ substantially from SM expectations. An important exception is  $\text{Br}(K_L \rightarrow \pi^0 \nu \bar{\nu})$ . This decay mode

	SM prediction	Exp. value
$\varepsilon$	$2.18 \times 10^{-3}$	$(2.282 \pm 0.017) \times 10^{-3}$
$ \delta m_B $	0.49	$0.489 \pm 0.008$
$a_{\psi K_S}$	0.71	$0.734 \pm 0.054$
$ \delta m_{B_s} $	17.6	$> 13.1$ (95%)
$ \delta m_D $	$\sim 10^{-5}$	$< 0.07$ (95%)
$\text{Br}(K^+ \rightarrow \pi^+ \nu \bar{\nu})$	$6.4 \times 10^{-11}$	$[3.2 - 48] \times 10^{-11}$ (90%)
$\text{Br}(K_L \rightarrow \mu^+ \mu^-)_{\text{SD}}$	$6.6 \times 10^{-10}$	$< 1.9 \times 10^{-9}$ (90%)
$\text{Br}(b \rightarrow s \gamma)$	$3.34 \times 10^{-4}$	$(3.3 \pm 0.4) \times 10^{-4}$
$\text{Br}(b \rightarrow s e^+ e^-)$	$7.3 \times 10^{-6}$	$< 11.0 \times 10^{-6}$ (90%)
$\text{Br}(b \rightarrow s \mu^+ \mu^-)$	$5.0 \times 10^{-6}$	$(8.9 \pm 2.7) \times 10^{-6}$
$\varepsilon'/\varepsilon$	$1.64 \times 10^{-3}$	$(1.72 \pm 0.18) \times 10^{-3}$

Table 5: Experimental values of the low energy observables used in the fits, together with the SM calculations with the parameters in Appendix A. The theoretical errors can be found in the text. The mass differences are in  $\text{ps}^{-1}$ .

does not provide a constraint yet, but in Models I and II it can have a branching ratio much larger than in the SM. Its analysis is postponed to Section 7.

## 6 Other constraints

The diagonal couplings of the  $u, d$  quarks to the  $Z$  boson are extracted from neutrino-nucleon scattering processes, atomic parity violation and the SLAC polarised electron experiment (see Ref. [5] and references therein for a more extensive discussion). The values of  $c_{L,R}^u, c_{L,R}^d$  derived from  $\nu N$  neutral processes have a large non-Gaussian correlation, and for the fit it is convenient to use instead

$$\begin{aligned}
g_L^2 &= \frac{1}{4} [(c_L^u)^2 + (c_L^d)^2], \\
g_R^2 &= \frac{1}{4} [(c_R^u)^2 + (c_R^d)^2], \\
\theta_L &= \arctan \frac{c_L^u}{c_L^d}, \\
\theta_R &= \arctan \frac{c_R^u}{c_R^d}.
\end{aligned} \tag{74}$$

The SM predictions for these parameters, including radiative corrections [5] and using the  $\overline{\text{MS}}$  definition of  $s_W^2$ , are collected in Table 6, together with their experimental values. The correlation matrix is in Table 7.

	SM prediction	Experimental measurement	Error
$g_L^2$	0.3038	0.3020	0.0019
$g_R^2$	0.0300	0.0315	0.0016
$\theta_L$	2.4630	2.50	0.034
$\theta_R$	5.1765	4.58	$^{+0.40}$ $^{-0.27}$

Table 6: SM calculation of  $g_L^2$ ,  $g_R^2$ ,  $\theta_L$ ,  $\theta_R$  and experimental values.

	$g_L^2$	$g_R^2$	$\theta_L$	$\theta_R$
$g_L^2$	1	0.32	-0.39	$\sim 0$
$g_R^2$	0.32	1	-0.10	$\sim 0$
$\theta_L$	-0.39	-0.10	1	0.27
$\theta_R$	$\sim 0$	$\sim 0$	0.27	1

Table 7: Correlation matrix for the parameters  $g_L^2$ ,  $g_R^2$ ,  $\theta_L$ ,  $\theta_R$ .

The interactions involved in atomic parity violation and the SLAC polarised electron experiment can be parameterised with the effective Lagrangian

$$\mathcal{L} = -\frac{G_F}{\sqrt{2}} \sum_{i=u,d} [C_{1i} \bar{e} \gamma_\mu \gamma^5 e \bar{q}_i \gamma^\mu q_i + C_{2i} \bar{e} \gamma_\mu e \bar{q}_i \gamma^\mu \gamma^5 q_i] \quad (75)$$

plus a QED contribution. We are not considering mixing of the leptons, and hence the coefficients  $C_{1i}$ ,  $C_{2i}$  are at tree level [19]

$$\begin{aligned} C_{1u} &= -\left(\frac{X_{uu}}{2} - \frac{4}{3}s_W^2\right), \\ C_{1d} &= -\left(-\frac{X_{dd}}{2} + \frac{2}{3}s_W^2\right), \\ C_{2u} &= X_{uu} \left(-\frac{1}{2} + 2s_W^2\right), \\ C_{2d} &= -X_{dd} \left(-\frac{1}{2} + 2s_W^2\right). \end{aligned} \quad (76)$$

The parameters  $C_{1u}$  and  $C_{1d}$  can be extracted from atomic parity violation measurements. The combination  $\tilde{C}_2 \equiv C_{2u} - C_{2d}/2$  is obtained in the polarised electron experiment. In Table 8 we quote the SM predictions of  $C_{1u}$ ,  $C_{1d}$ ,  $\tilde{C}_2$ , including the radiative corrections to Eqs. (76), and the experimental values. The correlation matrix is in Table 9.

	SM prediction	Experimental measurement	Error
$C_{1u}$	-0.1886	-0.209	0.041
$C_{1d}$	0.3413	0.358	0.037
$\tilde{C}_2$	-0.0492	-0.04	0.12

Table 8: Experimental values and SM calculations of the parameters  $C_{1u}$ ,  $C_{1d}$  in the Lagrangian in Eq. (75) and the combination  $\tilde{C}_2 = C_{2u} - C_{2d}/2$ .

	$C_{1u}$	$C_{1d}$	$\tilde{C}_2$
$C_{1u}$	1	-0.9996	-0.78
$C_{1d}$	-0.9996	1	0.78
$\tilde{C}_2$	-0.78	0.78	1

Table 9: Correlation matrix for the parameters  $C_{1u}$ ,  $C_{1d}$  and  $\tilde{C}_2 = C_{2u} - C_{2d}/2$ .

The leading effect of mixing with singlets is a decrease of  $X_{uu}$  (in Model I) and  $X_{dd}$  (in Model II), which reduces  $g_L^2$  and the modulus of  $\tilde{C}_2$  in both cases, and also the modulus of  $C_{1u}$  or  $C_{1d}$ , depending on the model considered. The angle  $\theta_L$  grows when the up quark mixes with a singlet and decreases when the mixing corresponds to the down quark. The right-handed couplings are not affected by mixing with singlets, and thus  $g_R^2$  and  $\theta_R$  remain equal to their SM values. However, they have to be included in the fit because of the experimental correlation. Another consequence of the mixing may possibly be the modification of the small radiative corrections to Eqs. (74,76). We neglect this subleading effect and assume that the corrections remain with their SM values.

# 7 Some observables from $K$ and $B$ physics with large new effects

There is a large number of observables of interest that will be tested in experiments under way and for which our models lead to departures from the SM. Necessarily, our study is not complete and we pass over many relevant processes that deserve further attention. We discuss for illustration the CP-violating decay  $K^0 \rightarrow \pi^0 \nu \bar{\nu}$  and the time-dependent CP asymmetry in  $B_s^0 \rightarrow D_s^+ D_s^-$ .

## 7.1 The decay $K^0 \rightarrow \pi^0 \nu \bar{\nu}$

This decay is closely related to  $K^+ \rightarrow \pi^+ \nu \bar{\nu}$ , but its detection is much more difficult. At present it is still unobserved, and the 90% CL limit on this decay mode is  $\text{Br}(K_L \rightarrow \pi^0 \nu \bar{\nu}) \leq 5.9 \times 10^{-7}$  [96]. It is calculated as

$$\begin{aligned} \text{Br}(K_L \rightarrow \pi^0 \nu \bar{\nu}) &= r_{K_L} \frac{\tau_{K_L}}{\tau_{K^+}} \text{Br}(K^+ \rightarrow \pi^0 e^+ \bar{\nu}) \frac{3\alpha^2}{2\pi^2 s_W^4 |V_{us}|^2} \\ &\times \left[ \eta_t^X X_0(x_t) \text{Im} \lambda_{sd}^t + \text{Im} \Delta_{K^+} \right]^2, \end{aligned} \quad (77)$$

with the corresponding isospin breaking correction  $r_{K_L} = 0.944$ . The SM prediction for this partial width is  $(2.3 \pm 0.17) \times 10^{-11}$ , one third of the value for  $\text{Br}(K^+ \rightarrow \pi^+ \nu \bar{\nu})$ . As only the imaginary parts of the CKM products enter in the expression for  $\text{Br}(K_L \rightarrow \pi^0 \nu \bar{\nu})$ , it is possible to have this decay rate much larger while keeping  $\text{Br}(K^+ \rightarrow \pi^+ \nu \bar{\nu})$  in agreement with experiment. However, there is a model-independent limit

$$\frac{\text{Br}(K_L \rightarrow \pi^0 \nu \bar{\nu})}{\text{Br}(K^+ \rightarrow \pi^+ \nu \bar{\nu})} \leq 4.376 \quad (78)$$

that holds provided lepton flavour is conserved [97]. We will find later that in our models this bound can be saturated, leading to a increase in  $\text{Br}(K_L \rightarrow \pi^0 \nu \bar{\nu})$  of an order of magnitude, even keeping  $\text{Br}(K^+ \rightarrow \pi^+ \nu \bar{\nu})$  at its SM value.

## 7.2 The CP asymmetry in $B_s^0 \rightarrow D_s^+ D_s^-$ .

The ‘‘gold plated’’ decay  $B_s^0 \rightarrow D_s^+ D_s^-$  is mediated by the quark-level transition  $\bar{b} \rightarrow \bar{c} c \bar{s}$ . This transition is dominated by a single tree-level amplitude  $A \propto V_{cb}^* V_{cs}$  and it is then free of hadronic uncertainties [98]. The time-dependent CP asymmetry is written



as  $a_{D_s^+ D_s^-} = \text{Im } \lambda_{D_s^+ D_s^-}$ , with [99]

$$\lambda_{D_s^+ D_s^-} = \frac{(M_{12}^{B_s})^*}{|M_{12}^{B_s}|} \frac{V_{cb} V_{cs}^*}{V_{cb}^* V_{cs}} \quad (79)$$

and also

$$a_{D_s^+ D_s^-} = \sin(2\zeta - 2\theta_{B_s}), \quad (80)$$

with

$$\zeta = \arg \left[ -\frac{V_{cb} V_{cs}^*}{V_{tb} V_{ts}^*} \right]. \quad (81)$$

and  $\theta_{B_s}$  parameterising the deviation of the phase of  $M_{12}^{B_s}$  with respect to its SM value,

$$2\theta_{B_s} = \arg \frac{M_{12}^{B_s}}{(M_{12}^{B_s})_{\text{SM}}}. \quad (82)$$

In the SM  $\zeta \simeq 0$ , so the asymmetry  $a_{D_s^+ D_s^-}$  is predicted to be very small ( $a_{D_s^+ D_s^-} \simeq 0.03$  with the parameters for the CKM matrix in Appendix A). Therefore, its measurement offers a good opportunity to probe new physics, which may manifest itself if a nonzero value is observed [99].

Another possible final state given by the same quark-level transition is  $\psi\phi$ . This state has a clean experimental signature at hadron colliders,  $\psi \rightarrow l^+ l^-$  and  $\phi \rightarrow K^+ K^-$ , providing better chances to measure  $\sin(2\zeta - 2\theta_{B_s})$  at Tevatron [100]. However, in this case both particles  $\psi$  and  $\phi$  have spin 1, and then the orbital angular momentum is not fixed. (In  $B_s^0 \rightarrow D_s^+ D_s^-$  the two  $D$  mesons have spin 0, and therefore they are produced in a  $l = 0$  CP-even state.) The  $\psi\phi$  are produced in an admixture of CP-even and CP-odd states, which can be disentangled with an analysis of the angular distribution of their decay products  $l^+ l^-$ ,  $K^+ K^-$  [101]. We will loosely refer to the CP asymmetries containing the phase  $(2\zeta - 2\theta_{B_s})$  as  $a_{D_s^+ D_s^-}$ , understanding that this includes the asymmetries corresponding to final states  $D_s^+ D_s^-$ ,  $\psi\phi$ ,  $D_s^{*+} D_s^{*-}$ , etc. Finally, it is worthwhile mentioning that  $\cos(2\zeta - 2\theta_{B_s})$  can also be measured, on condition that the width difference between the two mass eigenstates is sizeable [102]. This can be done without the need of tagging the initial state ( $B_s^0$  or  $\bar{B}_s^0$ ) and provides an independent measurement of this important phase.

## 8 Results

We are more interested in the departures from SM predictions originated by mixing with exotic singlets than in finding the best fit to all experimental data. Therefore

we must specify the criteria for what we will consider as agreement of these models with experiment, and of course our predictions depend on this choice. We require: (i) individual agreement of observables with data, and (ii) that the joint  $\chi^2$  of the observables, divided in subsets, is not much worse than the  $\chi^2$  of these subsets in the SM. For the first condition, the number of standard deviations allowed in a single observable is similar to the departure already present in the SM. The second condition consists in requiring that the  $\chi^2$  of a group of variables is smaller or equal to the SM  $\chi^2$  value increased by a quantity numerically equal to the number of variables in the group. In average, this condition means admitting a  $1\sigma$  deviation for a variable which in the SM coincides with the experimental measurement, an extra departure of  $0.41\sigma$  for a variable which is at  $1\sigma$  within the SM, or  $0.24\sigma$  for a variable which is already at  $2\sigma$  in the SM. This second condition is in practice much stronger than the first one. These criteria are best explained by enumerating them:

- The moduli of the CKM angles  $V_{ud}, V_{us}, V_{ub}, V_{cd}, V_{cs}, V_{cb}$  can be at most  $2\sigma$  away from the figures in Table 1. The sum of the  $\chi^2$  must be smaller than the SM result plus six.
- The predictions for  $R_b, R_c, A_{\text{FB}}^{0,b}, A_{\text{FB}}^{0,c}, \mathcal{A}_b, \mathcal{A}_c$  may be up to  $3\sigma$  away from the central values in Table 2. We allow larger departures than in the previous case because the SM prediction of  $A_{\text{FB}}^{0,b}$  is almost  $3\sigma$  from the experimental measurement. We also require that the  $\chi^2$  (calculated with the correlation matrix in Table 3) is smaller than the SM result plus four (in Model I) or plus three (in Model II). The number of variables in this subset that effectively change with the mixing are four and three in Models I and II, respectively.
- The contributions to the oblique parameters  $S, T, U$  from new physics have to be within  $2\sigma$  of the values in Table 4. The sum of the  $\chi^2$  of the three variables must be smaller than the SM  $\chi^2$  value plus three.
- The observables  $\varepsilon, |\delta m_B|$  and  $a_{\psi K_S}$  are allowed to move within  $2.5\sigma$  of the numbers in Table 5. The total  $\chi^2$  has to be smaller than the SM value plus three.
- The branching fractions for  $b \rightarrow s\gamma$  and  $b \rightarrow s\mu^+\mu^-$  are required to agree with the experimental figures in Table 5 within  $2\sigma$ , and their  $\chi^2$  has to be smaller than the SM result plus two.
- The departure of  $\varepsilon'/\varepsilon$  from the experimental measurement in Table 5 can be at most  $1\sigma$  larger than the departure within the SM.

- The parameters  $g_L^2, g_R^2, \theta_L, \theta_R, C_{1u}, C_{1d}$  and  $\tilde{C}_2$  have to be within  $2\sigma$  of the central values in Tables 6 and 8. Their  $\chi^2$  computed with the correlation matrices in Tables 7 and 9 is required to be smaller than the SM value plus five ( $g_R$  and  $\theta_R$  are not affected by the mixing in these models).

The observables  $\varepsilon$ ,  $|\delta m_B|$ ,  $\text{Br}(b \rightarrow s\gamma)$  and  $\varepsilon'/\varepsilon$  have large theoretical errors that are of similar magnitude as the experimental ones. In the comparison of these observables with experiment we use the prescription explained in Appendix C, assuming that the theoretical errors are Gaussian. For  $|\delta m_D|$ ,  $\text{Br}(K^+ \rightarrow \pi^+ \nu \bar{\nu})$ ,  $\text{Br}(K_L \rightarrow \mu^+ \mu^-)_{\text{SD}}$  and  $\text{Br}(b \rightarrow se^+e^-)$  we require that the predictions are in the experimental intervals quoted in Table 5 (the upper limit of  $|\delta m_D|$  in the literature has a 95% CL, instead of the more common one of 90%). We also set the condition  $|\delta m_{B_s}/\delta m_B| \geq 26.7$ , rather than  $|\delta m_{B_s}| > 13.1 \text{ ps}^{-1}$ , to avoid theoretical uncertainties. With all these restrictions we explore the parameter space to find the interval of variation of charged current top couplings, flavour-diagonal and flavour-changing  $Z$  couplings and the observables introduced in last Section. We discuss the results for Models I and II separately.

## 8.1 Mixing with an up singlet

One fundamental parameter in Model I is the mass of the new quark  $m_T$ . We find that for low  $m_T$  the effects of mixing can be huge, with  $V_{td}$ ,  $V_{ts}$  and  $V_{tb}$  very different from the SM predictions. In this scenario the effects of mixing on  $R_b$  and oblique corrections almost cancel, while the new quark can virtually take the place of the top in reproducing the experimental values of the meson observables analysed. This is viable because for small  $m_T$  the Inami-Lim functions for the top and the new quark are alike. As  $m_T$  grows this possibility disappears and the dominant contributions come from the top, but still significant departures from the SM can be found. In our analysis we have checked that for the values and plots shown the Yukawa couplings remain perturbative. The decoupling limit is not reached in any of the cases considered.

One of the most striking results in Model I is the deviation of  $|V_{tb}|$  from unity (see Fig. 1). The modulus of  $V_{tb}$  is determined by the coupling  $V_{Tb}$  in Fig. 2, and the latter is bounded by the  $T$  parameter, as it was seen in Section 4. (The dependence on only one observable leads to the very simple behaviour of the curves in Figs. 1 and 2.) For  $m_T = 200 \text{ GeV}$ ,  $|V_{tb}|$  can be as small as 0.58. The lower limit on  $|V_{tb}|$  grows with  $m_T$ , but even for  $m_T = 600 \text{ GeV}$  it is  $|V_{tb}| \geq 0.977$ , substantially different from the SM prediction  $|V_{tb}| = 0.999$ . Although sizeable and theoretically very important, this 2%

difference is difficult to detect experimentally at LHC, which is expected to measure the size of  $V_{tb}$  with a precision of  $\pm 0.07$  [13].

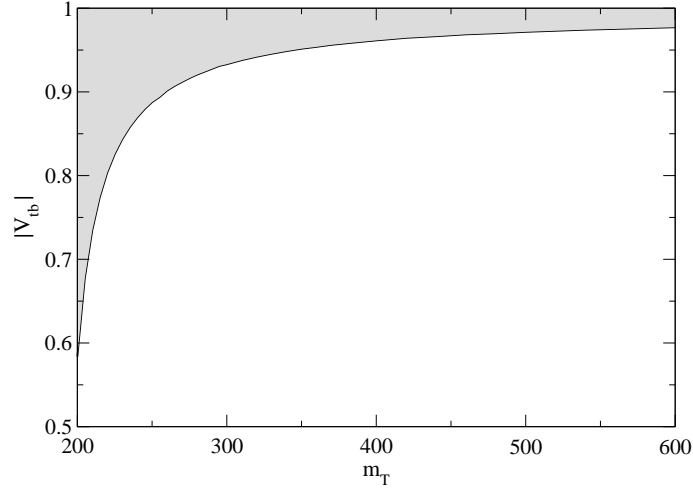


Figure 1: Allowed values of  $|V_{tb}|$  (shaded area) in Model I, as a function of the mass of the new quark.

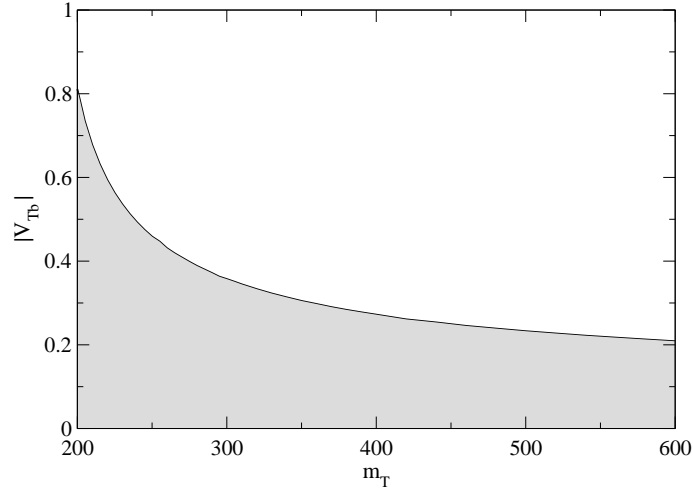


Figure 2: Allowed values of the coupling  $|V_{Tb}|$  of the new quark (shaded area) in Model I, as a function of its mass.

The top charged-current couplings  $V_{ts}$  and  $V_{td}$  can be very different from SM expectations as well. In the SM  $3 \times 3$  CKM unitarity fixes  $|V_{ts}| \simeq |V_{cb}|$ . In Model I  $|V_{ts}|$  can be between 0.002 and 0.061 for  $m_T = 200$  GeV (see Fig. 3). The allowed interval

narrows as  $m_T$  increases, and for  $m_T = 600$  GeV the interval is essentially the same as in the SM. The range of variation of  $V_{td}$  is also considerably greater than in the SM (see Fig. 4). For  $m_T \leq 300$  GeV  $V_{td}$  can be almost zero (and in this case the  $T$  quark would account for the measured values of  $K$  and  $B$  observables), or even larger than  $V_{ts}$ , as can be seen in Fig. 5. Again, for heavier  $T$  the permitted interval decreases and for  $m_T = 600$  GeV it is practically the same interval as in the SM. We remark that the curves in Figs. 3-5 giving the upper and lower bounds arise from the various restrictions discussed in Sections 3-6, especially those regarding meson observables, thus their complicated behaviour should not be surprising. We do not claim that the blank regions in these three figures are excluded. The quoted allowed limits might be wider if some delicate cancellation not found in the numerical analysis allows a small region in parameter space with  $V_{td}$ ,  $V_{ts}$  or their ratio outside the shaded areas.

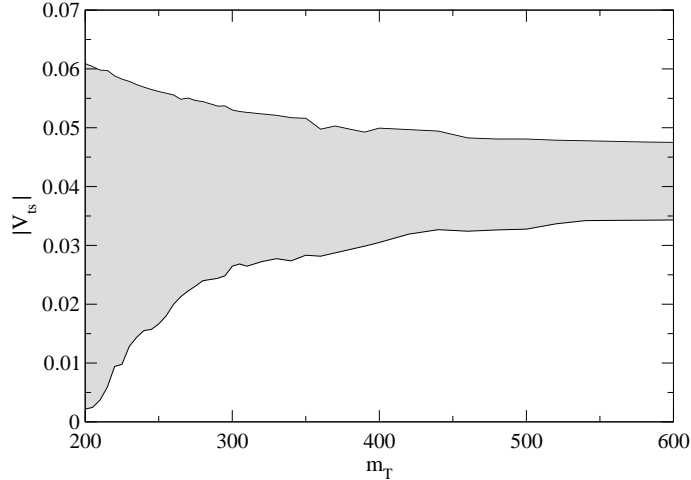


Figure 3: Allowed values of  $|V_{ts}|$  (shaded area) in Model I, as a function of the mass of the new quark.

In contrast with the former, the intervals for CKM mixing angles  $V_{Td}$ ,  $V_{Ts}$  do not show a pronounced decrease with  $m_T$ .  $V_{Td}$  can be in the interval  $0 \leq |V_{Td}| \leq 0.05$  for the  $m_T$  values studied, and the maximum size of  $|V_{Ts}|$  decreases from 0.06 for  $m_T = 200$  to 0.05 for  $m_T = 600$  GeV.

The counterpart of the departure from the SM prediction  $|V_{tb}| = 0.999$  is the decrease of the  $Ztt$  coupling. Within the SM, the isospin-related term  $X_{tt}$  equals one by the GIM mechanism, while in Model I the GIM breaking originated by mixing with a singlet reduces its magnitude. The modulus of  $X_{tt}$ , as well as  $V_{tb}$ , is determined by the parameter  $V_{Tb}$  and hence its possible size is dictated only by the  $T$  parameter. The

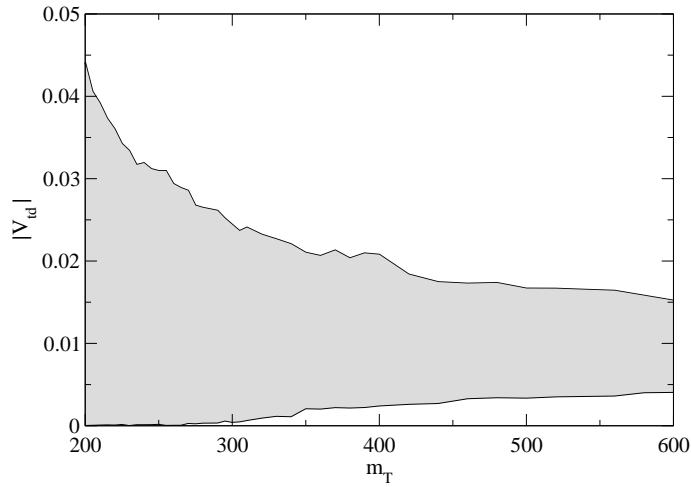


Figure 4: Allowed values of  $|V_{td}|$  (shaded area) in Model I, as a function of the mass of the new quark.

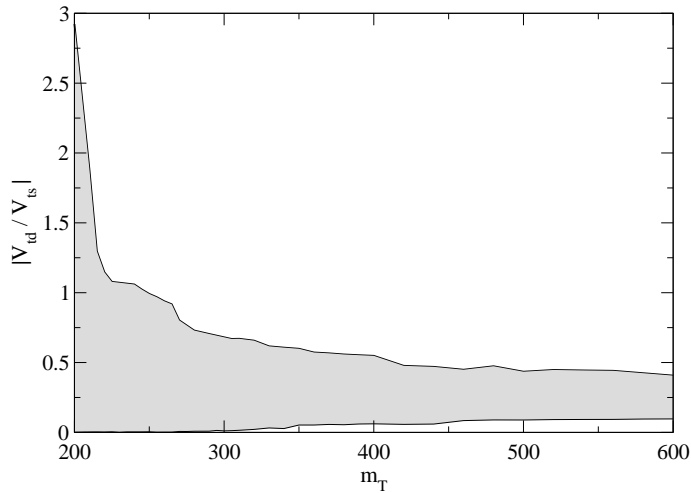


Figure 5: Allowed values of the ratio  $|V_{td}/V_{ts}|$  (shaded area) in Model I, as a function of the mass of the new quark.

interval allowed for  $X_{tt}$  is plotted in Fig. 6, where we observe that for  $m_T = 200$  GeV it reaches down to  $X_{tt} = 0.34$ . The lower limit of the interval grows with  $m_T$  and is approximately  $X_{tt} = 0.96$  for  $m_T = 600$  GeV. The  $Ztt$  coupling will be precisely measured in  $t\bar{t}$  production at TESLA. With a CM energy of 500 GeV and an integrated luminosity of  $300 \text{ fb}^{-1}$ , 34800 top pairs are expected to be collected at the detector in the semileptonic channel  $l\nu jjjj$ , with  $l$  an electron or a muon. The estimated preci-

sion in the determination of  $X_{tt}$  with this channel alone is of 0.02. Then, even with  $m_T = 600$  GeV a  $2\sigma$  effect could be visible.

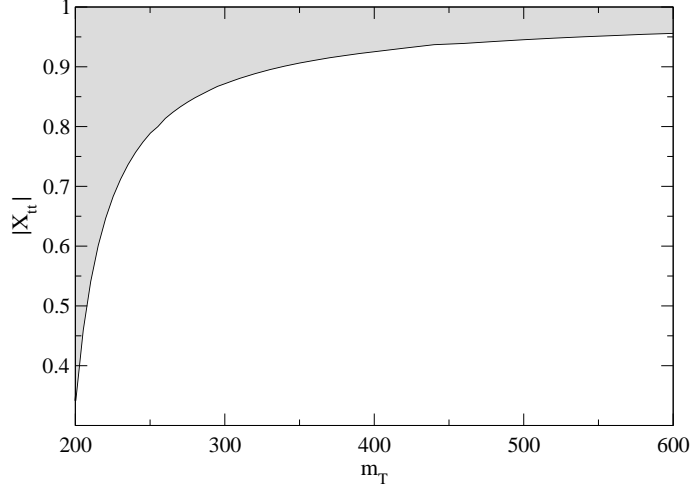


Figure 6: Allowed values of  $|X_{tt}|$  (shaded area) in Model I, as a function of the mass of the new quark.

FCN couplings are perhaps the most conspicuous manifestation of mixing with quark singlets, and offer another excellent place to search for new physics. In the SM they vanish at tree-level by the GIM mechanism, and the effective vertices generated at one loop are very small as a consequence of the GIM suppression [103]. This results in a negligible branching ratio  $\text{Br}(t \rightarrow Zc) \sim 10^{-14}$  within the SM. In Model I the FCN coupling  $X_{ct}$  can be sizeable [39], leading to top decays  $t \rightarrow Zc$  [104],  $Zt$  production at LHC [105, 106] and single top production at linear colliders [107, 108, 109, 110]. For  $m_T \sim m_t$  the new contributions to meson observables involving  $T$  diagrams are small, and this FCN coupling can be relatively large,  $|X_{ct}| = 0.036$  (see Fig. 7) <sup>6</sup>. A coupling of this size yields a branching ratio  $\text{Br}(t \rightarrow Zc) = 6.0 \times 10^{-4}$  (nine orders of magnitude above the SM prediction) that would be seen at LHC with  $18\sigma$  statistical significance in top decays and  $4.6\sigma$  in  $Zt$  production (with an integrated luminosity of  $100 \text{ fb}^{-1}$ ), and at TESLA with  $8.2\sigma$  significance in single top production (with  $300 \text{ fb}^{-1}$ ). For larger  $m_T$ , the contributions of the  $T$  quark to meson observables (in particular to  $K^+ \rightarrow \pi^+ \nu \bar{\nu}$  and the short-distance part of  $K_L \rightarrow \mu^+ \mu^-$ ) decrease monotonically the upper limit on  $|X_{ct}|$ , with some very small local “enhancements” that can be observed

<sup>6</sup>The reduction with respect to the number quoted in Ref. [39] is mainly due to the improved limit on  $|\delta m_D|$ .

in Fig. 7. For  $T$  very heavy there is still the possibility of  $|X_{ct}| = 0.009$ , giving  $\text{Br}(t \rightarrow Zc) = 3.8 \times 10^{-5}$ , which would have a  $1.2\sigma$  significance in top decay processes at LHC.

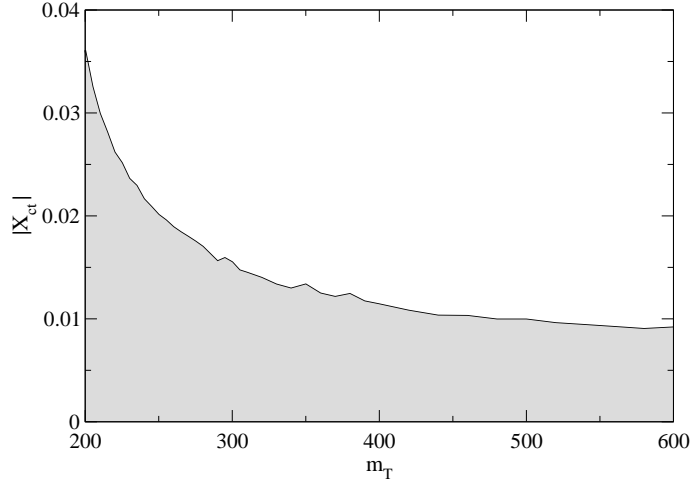


Figure 7: Allowed values of the FCN coupling  $|X_{ct}|$  (shaded area) in Model I, as a function of the mass of the new quark.

In Model I the  $X_{ut}$  coupling can have the same size as  $X_{ct}$ . This contrasts with other SM extensions (for instance, SUSY or two Higgs doublet models) where observable FCN  $tc$  vertices can be generated but  $tu$  vertices are suppressed. The observability of a  $Ztu$  FCN coupling is the same, and even better in the case of  $Zt$  production processes at LHC. The coupling  $X_{tT}$  between the top and the new mass eigenstate (which is a function of the charged-current coupling  $V_{Tb}$ ) can reach the maximum value permitted by the model,  $X_{tT} = 0.5$  for  $m_T \leq 210$  GeV, descending slowly to a maximum of  $X_{tT} = 0.2$  when  $m_T = 600$  GeV.

The mixing with a new singlet may also give new effects in low energy observables. The branching ratio of  $K_L \rightarrow \pi^0 \nu \bar{\nu}$  can reach  $2 \times 10^{-10}$  for “low”  $m_T$ , and  $4.4 \times 10^{-10}$  for  $m_T \geq 300$  GeV, one order of magnitude above the SM prediction  $\text{Br}(K_L \rightarrow \pi^0 \nu \bar{\nu}) = 2.4 \times 10^{-11}$ . These rates would be visible already at the E391 experiment at KEK, which aims at a sensitivity of  $3 \times 10^{-10}$ , and up to  $\sim 10^3$  events could be collected at the KOPIO experiment approved for construction at BNL (for a summary of the prospects on the rare decays  $K^+ \rightarrow \pi^+ \nu \bar{\nu}$  and  $K_L \rightarrow \pi^0 \nu \bar{\nu}$  see for instance Ref. [111]). The ratio  $\text{Br}(K_L \rightarrow \pi^0 \nu \bar{\nu})/\text{Br}(K^+ \rightarrow \pi^+ \nu \bar{\nu})$  of the decay rates of the two kaon “golden modes”, plotted in Fig. 9, can be enhanced an order of magnitude over the SM prediction  $\sim 0.35$ , and saturate the limit in Eq. (78) for  $m_T \geq 310$  GeV. This enhancement and a larger



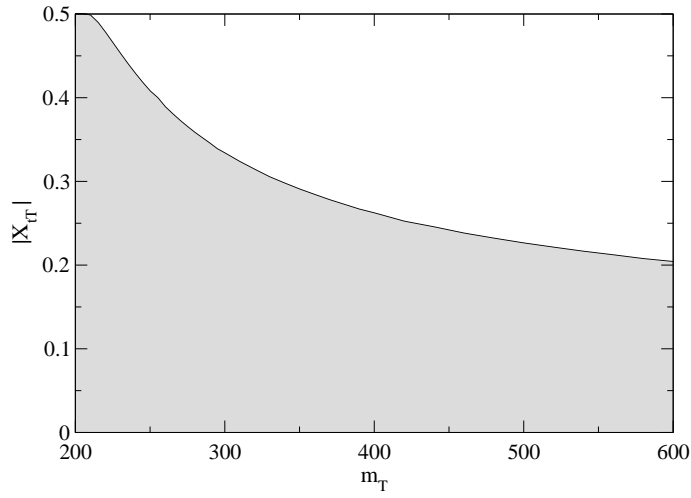


Figure 8: Allowed values of the coupling  $|X_{tT}|$  of the new quark (shaded area) in Model I, as a function of its mass.

value of  $\text{Br}(K^+ \rightarrow \pi^+ \nu \bar{\nu})$  (compatible with experimental data) lead to the maximum value  $\text{Br}(K_L \rightarrow \pi^0 \nu \bar{\nu}) = 4.4 \times 10^{-10}$ . On the other hand, a strong suppression of this decay mode is possible, with values several orders of magnitude below the SM prediction.

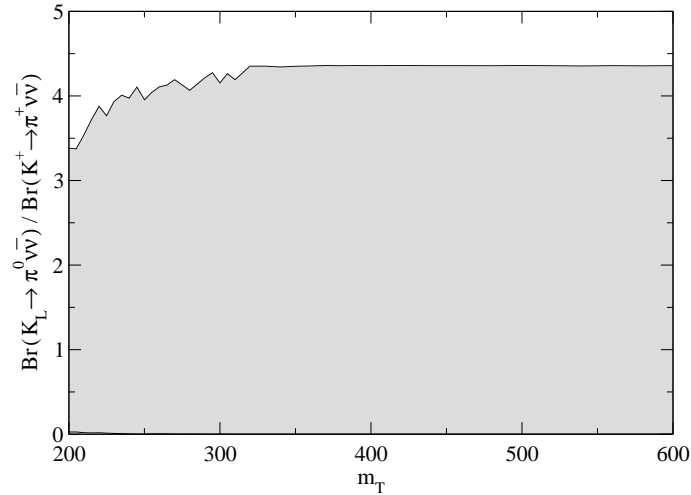


Figure 9: Range of variation of  $\text{Br}(K_L \rightarrow \pi^0 \nu \bar{\nu}) / \text{Br}(K^+ \rightarrow \pi^+ \nu \bar{\nu})$  in Model I (shaded area).

The mass difference in the  $B_s$  system is predicted to be  $\sim 18 \text{ ps}^{-1}$  within the SM.

The existing lower bound  $|\delta m_{B_s}| \geq 13.1 \text{ ps}^{-1}$  can be saturated in practically all the interval of  $m_T$  studied. The ratio  $|\delta m_{B_s}/\delta m_{B_d}|$  has been proposed for a determination of  $|V_{ts}/V_{td}|$  [5]. Of course, this determination is strongly model-dependent, because new physics may contribute to both mass differences. This ratio equals 36 in the SM, and in Model I it may have values between the experimental lower limit of 26.7 and 77. Finally, the asymmetry  $a_{D_s^+ D_s^-}$ , which practically vanishes in the SM, provides a crucial test of the phase structure of the CKM matrix. The non-unitarity of the  $3 \times 3$  CKM submatrix and the presence of extra CP violating phases in Model I allow the asymmetry  $a_{D_s^+ D_s^-}$  to vary between  $-0.4$  and  $0.4$  for  $m_T \geq 275 \text{ GeV}$ , as can be observed in Fig. 10.

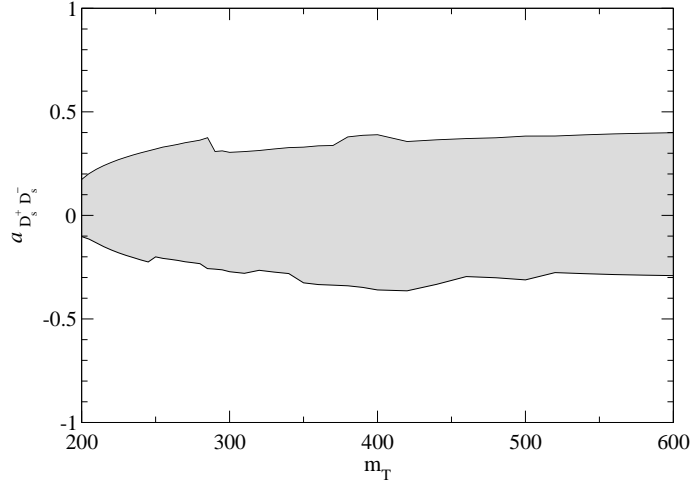


Figure 10: Range of variation of  $a_{D_s^+ D_s^-}$  in Model I (shaded area).

## 8.2 Mixing with a down singlet

In Model II the mass of the new quark does not play an important rôle in the constraints on the parameters of the model. The only dependence on  $m_B$  appears in the  $D^0$  mass difference (which at present does not imply any restriction at least for masses up to 1 TeV),  $b \rightarrow s\gamma$  (less restrictive than  $b \rightarrow sl^+l^-$ ) and oblique parameters, which are less important than  $R_b$  and have no influence in practice. Agreement of the latter with experiment requires that  $|V_{tb}|$  is very close to unity,  $|V_{tb}| \geq 0.998$ . This is indistinguishable from the SM prediction  $|V_{tb}| = 0.999$ , and forces  $V_{td}$  and  $V_{ts}$  to be within the SM range,  $0.0059 \leq |V_{td}| \leq 0.013$ ,  $0.035 \leq |V_{ts}| \leq 0.044$ . The CKM

matrix elements involving the new quark are all small,  $|V_{uB}| \leq 0.087$ ,  $|V_{cB}| \leq 0.035$ ,  $|V_{tB}| \leq 0.041$ , but noticeably they can be larger than  $V_{ub}$ .

FCN couplings between the light quarks are small (as required by low energy observables), especially the coupling between the  $d$  and  $s$  quarks,  $|X_{ds}| \leq 1.0 \times 10^{-5}$ . It makes sense to study  $\text{Re } X_{ds}$  and  $\text{Im } X_{ds}$  separately, even though in principle  $X_{ds}$  is not a rephasing-invariant quantity. This is so because Eq. (38) assumes a CKM parameterisation with  $V_{ud}^* V_{us}$  real. This requirement eliminates the freedom to rephase  $X_{ds}$  (up to a minus sign) and enables to separate its real and imaginary parts meaningfully. The region of allowed values for  $X_{ds}$  is plotted in Fig. 11 for comparison with other analyses in the literature [36, 37, 38]. This figure must be interpreted with care: the density of points is not associated to any meaning of “probability”, but it is simply an effect related to the random generation and CKM parameterisation used to obtain the data points, and the finiteness of the sample. The height of the allowed area is determined by the  $\varepsilon'/\varepsilon$  constraint, and the width by  $K_L \rightarrow \mu^+ \mu^-$ . Comparing this plot with the ones in Refs. [36, 38] we see that the left part of the rectangle determined by  $\varepsilon'/\varepsilon$  and  $K_L \rightarrow \mu^+ \mu^-$  is practically eliminated by the constraints from  $K^+ \rightarrow \pi^+ \nu \bar{\nu}$  and  $\varepsilon$ , except the upper left corner. The height of the rectangle is also smaller, meaning that in our case the requirement from  $\varepsilon'/\varepsilon$  (using the prescription in Appendix C) is more stringent.

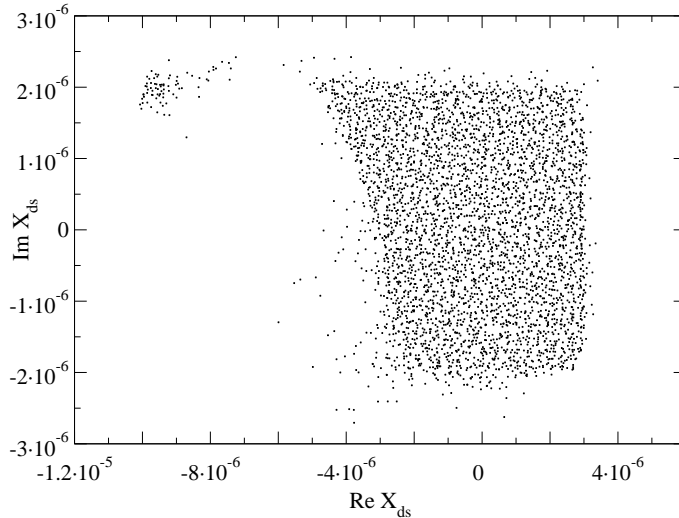


Figure 11: Allowed region for the real and imaginary parts of the FCN coupling  $X_{ds}$  in Model II.

The upper bounds for  $X_{db}$  and  $X_{sb}$  found in our analysis are  $|X_{db}| \leq 1.1 \times 10^{-3}$ ,

$|X_{sb}| \leq 1.1 \times 10^{-3}$ . Plots analogous to Fig. 11 are not meaningful for these parameters, because there is a freedom to rephase the  $b$  field and change arbitrarily the phases of  $X_{db}$  and  $X_{sb}$ . The only meaningful bounds are hence the limits on their moduli. The FCN coupling  $X_{bB}$  is not so limited by low energy measurements, and can reach 0.041.

Despite these restrictions on  $X_{ds}$ ,  $X_{db}$ ,  $X_{sb}$  and the fact that CKM matrix elements involving the known quarks must be within the SM range, the presence of tree-level FCN couplings has sizeable effects on some low energy observables, of the same magnitude as in Model I. A decay rate  $\text{Br}(K_L \rightarrow \pi^0 \nu \bar{\nu}) = 1.6 \times 10^{-10}$  can be achieved, and the ratio  $\text{Br}(K_L \rightarrow \pi^0 \nu \bar{\nu})/\text{Br}(K^+ \rightarrow \pi^+ \nu \bar{\nu})$  can equal 4.34. The lower limit on  $|\delta m_{B_s}|$  can be saturated, and the ratio  $|\delta m_{B_s}/\delta m_{B_d}|$  can be up to 67. On the other hand, the asymmetry  $a_{D_s^+ D_s^-}$  takes values between  $-3 \times 10^{-3}$  and 0.11. This upper limit is a factor of 2 – 3 larger than the SM prediction.

### 8.3 Mixing with two singlets

Mixing with more than one singlet lets two quarks of the same charge, for instance the  $d$  and  $s$  quarks, mix significantly with exotic quarks without necessarily generating a FCN coupling  $X_{ds}$  between them, in virtue of Eqs. 9. This allows a better fit to the measured CKM matrix elements and  $u$ ,  $d$  diagonal couplings to the  $Z$  boson, especially in Model II. In this model the global fit can be considerably better than in the SM, for instance with the CKM matrix

$$\begin{aligned}
 |V| &= \begin{pmatrix} 0.9742 & 0.2187 & 0.0037 & 0.0325 & 0.0442 \\ 0.2183 & 0.9750 & 0.0401 & 0.0076 & 0.0097 \\ 0.0074 & 0.0396 & 0.9992 & 0.0061 & 0.0036 \\ 0.0539 & 0.0001 & 0.0028 & 0.7370 & 0.6737 \\ 0.0160 & 0.0002 & 0.0066 & 0.6750 & 0.7376 \end{pmatrix}, \\
 \arg V &= \begin{pmatrix} 0.00 & 0.00 & 3.09 & 0.00 & 0.00 \\ 5.63 & 2.49 & 0.28 & 5.66 & 5.61 \\ 1.79 & 5.36 & 0.00 & 0.02 & 2.92 \\ 0.69 & 2.56 & 0.00 & 3.60 & 4.02 \\ 3.96 & 2.70 & 0.00 & 2.91 & 0.19 \end{pmatrix}. \tag{83}
 \end{aligned}$$

The actual masses of the two extra down quarks are not very relevant, and have been taken as 200 and 400 GeV in the calculation. In this example the  $\chi^2$  of the six measured CKM matrix elements is 1.14, while in the SM best fit it is 4.77. The parameters describing the  $Zuu$  and  $Zdd$  couplings are  $g_L^2 = 0.3024$ ,  $\theta_L = 2.4612$ ,  $C_{1d} = 0.3398$ ,

$\tilde{C}_2 = -0.0492$ , and the others unchanged with respect to their SM values. The  $\chi^2$  of these parameters is 7.73, improving the SM value of 10.5. The agreement of the rest of the observables with experiment is equal or better than within the SM, as can be seen in Table 10 (the experimental results for  $\varepsilon$  and  $\delta m_B$  can be accommodated with slightly larger  $\hat{B}$  parameters). This example of “best fit” matrix gives the predictions  $|X_{bB}| = 0.006$ ,  $|X_{bB'}| = 0.004$ . The result  $\text{Br}(K_L \rightarrow \pi^0 \nu \bar{\nu}) = 2.0 \times 10^{-10}$  is very similar to the SM case, but other examples with a little worse  $\chi^2$  can be found, having enhancements (or suppressions) of this rate by factors up to three. These examples show explicitly that new physics effects are not in contradiction with good agreement with experimental data, although our restrictive criteria for agreement with experiment at the beginning of this Section already made it apparent.

Observable	Value
$R_b$	0.21590
$R_c$	0.1724
$A_{\text{FB}}^{0,b}$	0.1039
$A_{\text{FB}}^{0,c}$	0.0744
$\mathcal{A}_b$	0.935
$\mathcal{A}_c$	0.669
$\varepsilon$	$2.08 \times 10^{-3}$
$ \delta m_B $	0.45
$ \delta m_{B_s} $	17.6
$a_{\psi K_S}$	0.74
$\text{Br}(K^+ \rightarrow \pi^+ \nu \bar{\nu})$	$6.0 \times 10^{-11}$
$\text{Br}(K_L \rightarrow \mu^+ \mu^-)_{\text{SD}}$	$6.3 \times 10^{-10}$
$\text{Br}(b \rightarrow s \gamma)$	$3.35 \times 10^{-3}$
$\text{Br}(b \rightarrow s e^+ e^-)$	$7.3 \times 10^{-6}$
$\text{Br}(b \rightarrow s \mu^+ \mu^-)$	$5.0 \times 10^{-6}$
$\varepsilon'/\varepsilon$	$1.6 \times 10^{-3}$

Table 10: Values of some observables for the “best fit” matrix in Model II with two extra singlets. The mass differences are in  $\text{ps}^{-1}$ .

Finally, we have also noticed that the predictions for the parameters and observables under study do not change appreciably neither in Model I nor in Model II when we allow mixing with more than one singlet of the same charge.

## 9 Conclusions

The aim of this paper has been to investigate how the existence of a new quark singlet may change many predictions of the SM while keeping agreement with present experimental data. In Model I the mixing with a  $Q = 2/3$  singlet might lead to huge departures from the SM expectation for the CKM matrix elements  $V_{td}$ ,  $V_{ts}$ ,  $V_{tb}$  and the diagonal coupling  $Z_{tt}$ . Additionally, observable FCN couplings  $Z_{tu}$  and  $Z_{tc}$  may appear. These effects depend on the mass of the new quark, as has been shown in Figs. 1-9. For  $m_T \sim 200$  GeV the new quark might effectively replace the top in reproducing the experimental observables in  $K$  and  $B$  physics, allowing for values of  $V_{td}$  and  $V_{ts}$  very different from the SM predictions. On the other hand, for larger  $m_T$  the leading contributions to  $K$  and  $B$  observables are the SM ones, with possible new contributions from the new quark. This effect can be clearly appreciated in Figs. 3–5, where it is also apparent how important a direct determination of  $V_{td}$  and  $V_{ts}$  would be. Unfortunately, the difficulty in tagging light quark jets at Tevatron and LHC makes these measurements very hard, if not impossible. Any experimental progress in this direction would be most welcome.

The mixing of the top with the new quark results in values of  $V_{tb}$  and the  $Z_{tt}$  coupling parameter  $X_{tt}$  significantly smaller than one. These deviations from unity would be observable at LHC [13] and TESLA, respectively. For larger  $m_T$ ,  $|V_{tb}|$  and  $|X_{tt}|$  must be closer to unity, as can be seen in Figs. 1 and 6. However, the decrease in  $X_{tt}$  would be visible at TESLA even for  $m_T = 600$  GeV. The FCN couplings  $Z_{tu}$  and  $Z_{tc}$  could also be observed at LHC for a wide range of  $m_T$  [104, 105, 106].

The effects of top mixing are not limited to large colliders. Indeed, the observables in  $K$  and  $B$  physics studied here provide an example where these effects do not disappear when the mass of the new quark is large. We have shown that the predictions for the decay  $K_L \rightarrow \pi^0 \nu \bar{\nu}$ , the  $\delta m_{B_s}$  mass difference and the CP asymmetry  $a_{D_s^+ D_s^-}$  can be very different from the SM expectations, and effects of new physics could be observed in experiments under way or planned. These predictions for Model I are collected in Table 11. Before LHC operation, indirect evidences of new physics could appear in the measurement of CP asymmetries at  $B$  factories. A good candidate is the asymmetry  $a_{D_s^+ D_s^-}$  discussed here, but many other observables and CP asymmetries are worth analysing. If no new physics is observed, further constraints could be placed on CP violating phases.

In Model II the effects of the new  $Q = -1/3$  singlet on CKM matrix elements are

Quantity	Range	
$ V_{tb} $	0.58	1
$ V_{td} $	$4 \times 10^{-5}$	0.044
$ V_{ts} $	0.002	0.06
$ V_{td}/V_{ts} $	$6 \times 10^{-4}$	2.9
$ V_{Td} $	0	0.052
$ V_{Ts} $	0	0.063
$ V_{Tb} $	0	0.81
$ X_{tt} $	0.34	1
$ X_{ut} $	0	0.038
$ X_{ct} $	0	0.036
$ X_{tT} $	0	0.5
$\text{Br}(K_L \rightarrow \pi^0 \nu \bar{\nu})$	$\sim 0$	$4.4 \times 10^{-10}$
$\frac{\text{Br}(K_L \rightarrow \pi^0 \nu \bar{\nu})}{\text{Br}(K^+ \rightarrow \pi^+ \nu \bar{\nu})}$	$\sim 0$	4.35
$ \delta m_{B_s} / \delta m_B $	26.7	77
$a_{D_s^+ D_s^-}$	-0.4	0.4

Table 11: Summary of the predictions for Model I.

negligible and FCN couplings between known quarks are very constrained by experimental data. However, the predictions for meson observables, summarised in Table 12, are rather alike. In addition, we have shown how the mixing with two singlets can improve the agreement with the experimental determination of CKM matrix elements and  $Zuu$ ,  $Zdd$  couplings. This can be done keeping similar and in some cases better agreement with electroweak precision data and  $K$  and  $B$  physics observables.

All the effects of mixing with singlets described are significant, but of course the decisive evidence would be the discovery of a new quark, which might happen at LHC or even at Tevatron, provided it exists and it is light enough. In this case, the pattern of new physics effects would allow to uncover its nature. Conversely, the non-observation of a new quark would be very important as well. If no new quark is found at LHC, the indirect constraints on CKM matrix elements and nonstandard contributions to meson physics would considerably improve.

Quantity	Range	
$ V_{tb} $	0.998	1
$ V_{td} $	0.0059	0.013
$ V_{ts} $	0.035	0.044
$ V_{ub} $	0	0.087
$ V_{cb} $	0	0.035
$ V_{tb} $	0	0.041
$ X_{ds} $	0	$1.0 \times 10^{-5}$
$\text{Re } X_{ds}$	$-1.0 \times 10^{-5}$	$3.4 \times 10^{-6}$
$\text{Im } X_{ds}$	$-2.7 \times 10^{-6}$	$2.4 \times 10^{-6}$
$ X_{db} $	0	$1.1 \times 10^{-3}$
$ X_{sb} $	0	$1.1 \times 10^{-3}$
$ X_{bB} $	0	0.041
$\text{Br}(K_L \rightarrow \pi^0 \nu \bar{\nu})$	$\sim 0$	$1.6 \times 10^{-10}$
$\frac{\text{Br}(K_L \rightarrow \pi^0 \nu \bar{\nu})}{\text{Br}(K^+ \rightarrow \pi^+ \nu \bar{\nu})}$	$\sim 0$	4.34
$ \delta m_{B_s} / \delta m_B $	26.7	67
$a_{D_s^+ D_s^-}$	$-3 \times 10^{-3}$	0.11

Table 12: Summary of the predictions for Model II.

## A Common input parameters

Unless otherwise specified, experimental data used throughout the paper are taken from Refs. [1, 5]. We use the results in Ref. [112] to convert the pole masses  $m_i$  to the  $\overline{\text{MS}}$  scheme and to perform the running to the scale  $M_Z$ . The results are in Table 13. For  $u, d, s$  we quote the  $\overline{\text{MS}}$  masses at 2 GeV instead of the pole masses. The numbers between brackets are not directly used in the calculations.

The running masses  $\overline{m}_c(\overline{m}_c) = 1.28$ ,  $\overline{m}_b(\overline{m}_b) = 4.19$  are also needed. The lepton pole masses are  $m_e = 0.511$  MeV,  $m_\mu = 0.105$  and  $m_\tau = 1.777$  GeV. We take  $M_Z = 91.1874$ ,  $\Gamma_Z = 2.4963$ ,  $M_W = 80.398$  and  $M_H = 115$  GeV. The electromagnetic and strong coupling constants at the scale  $M_Z$  are  $\alpha = 1/128.878$ ,  $\alpha_s = 0.118$ . The sine of the weak angle in the  $\overline{\text{MS}}$  scheme is  $s_Z^2 = 0.23113$ .

The CKM matrix used in the context of the SM is obtained by a fit to the six measured moduli in Table 1, and is determined by  $|V_{us}| = 0.2224$ ,  $|V_{ub}| = 0.00362$ ,  $|V_{cb}| = 0.0402$ , and the rest of the elements obtained using  $3 \times 3$  unitarity. The phase



	$m_i$	$\overline{m}_i(m_i)$	$\overline{m}_i(M_Z)$
$m_u$	(0.003)	–	0.0016
$m_d$	(0.006)	–	0.0033
$m_c$	1.5	1.22	0.68
$m_s$	0.12	–	0.067
$m_t$	174.3	164.6	175.6
$m_b$	4.7	4.12	2.9

Table 13: Quark masses (in GeV) used in the evaluations. The uncertainty in  $m_t$  is taken as  $\pm 5.1$  GeV. For  $u, d, s$  we write the  $\overline{\text{MS}}$  masses  $\overline{m}_i(2 \text{ GeV})$  instead of the pole masses.

$\delta$  in the standard parameterisation [5] is determined performing a fit to  $\varepsilon, \varepsilon'/\varepsilon, a_{\psi K_S}$  and  $|\delta m_B|$  with the rest of parameters quoted, and the result  $\delta = 1.014$  is very similar to the one obtained in the fit in Ref. [5].

## B Inami-Lim functions

In this Appendix we collect the Inami-Lim functions used in Section 5. The box functions  $F$  and  $S_0$  appear in meson oscillations.  $D'_0, E_0$  and  $E'_0$  are related to photon and gluon penguins. The functions  $X_0$  and  $Y_0$  are gauge-invariant combinations of the box function  $B_0$  and the  $Z$  penguin function  $C_0$ ,  $X_0 = C_0 - 4B_0$ ,  $Y_0 = C_0 - B_0$ . The function  $Z_0$  is a gauge-invariant combination of photon and  $Z$  penguins. Their expressions read [56, 57]

$$E_0(x_i) = -\frac{2}{3} \log x_i + \frac{x_i(18 - 11x_i - x_i^2)}{12(1 - x_i)^3} + \frac{x_i^2(15 - 16x_i + 4x_i^2)}{6(1 - x_i)^4} \log x_i, \quad (84)$$

$$D'_0(x_i) = -\frac{8x_i^3 + 5x_i^2 - 7x_i}{12(1 - x_i)^3} + \frac{-3x_i^3 + 2x_i^2}{2(1 - x_i)^4} \log x_i, \quad (85)$$

$$E'_0(x_i) = -\frac{x_i^3 - 5x_i^2 - 2x_i}{4(1 - x_i)^3} + \frac{3x_i^2}{2(1 - x_i)^4} \log x_i, \quad (86)$$

$$F(x_i, x_j) = \frac{4 - 7x_i x_j}{4(1 - x_i)(1 - x_j)} + \frac{4 - 8x_j + x_i x_j}{4(1 - x_i)^2(x_i - x_j)} x_i^2 \log x_i \\ + \frac{4 - 8x_i + x_i x_j}{4(1 - x_j)^2(x_j - x_i)} x_j^2 \log x_j, \quad (87)$$

$$S_0(x_i, x_j) = -\frac{3x_i x_j}{4(x_i - 1)(x_j - 1)} + \frac{x_i x_j (x_i^2 - 8x_i + 4)}{4(x_i - 1)^2(x_i - x_j)} \log x_i$$

$$+ \frac{x_i x_j (x_j^2 - 8x_j + 4)}{4(x_j - 1)^2(x_j - x_i)} \log x_j, \quad (88)$$

$$S_0(x_i) = \frac{4x_i - 11x_i^2 + x_i^3}{4(1 - x_i)^2} - \frac{3x_i^3}{2(1 - x_i)^3} \log x_i, \quad (89)$$

$$Z_0(x_i) = -\frac{1}{9} \log x_i + \frac{18x_i^4 - 163x_i^3 + 259x_i^2 - 108x_i}{144(x_i - 1)^3} + \frac{32x_i^4 - 38x_i^3 - 15x_i^2 + 18x_i}{72(x_i - 1)^4} \log x_i, \quad (90)$$

$$B_0(x_i) = \frac{1}{4} \left[ \frac{x_i}{1 - x_i} + \frac{x_i}{(x_i - 1)^2} \log x_i \right], \quad (91)$$

$$C_0(x_i) = \frac{x_i}{8} \left[ \frac{x_i - 6}{x_i - 1} + \frac{3x_i + 2}{(x_i - 1)^2} \log x_i \right], \quad (92)$$

$$X_0(x_i) = \frac{x_i}{8} \left[ \frac{x_i + 2}{x_i - 1} + \frac{3x_i - 6}{(x_i - 1)^2} \log x_i \right], \quad (93)$$

$$Y_0(x_i) = \frac{x_i}{8} \left[ \frac{x_i - 4}{x_i - 1} + \frac{3x_i}{(x_i - 1)^2} \log x_i \right]. \quad (94)$$

The functions appearing in the  $Z$  FCNC penguins involved in the calculation of  $b \rightarrow s\gamma$  are [81]

$$\xi_s^Z = \frac{1}{54}(-3 + 2s_W^2), \quad (95)$$

$$\xi_b^Z = \frac{1}{54}(-3 - 4s_W^2), \quad (96)$$

$$\xi_B^Z(y_B) = -\frac{8 - 30y_B + 9y_B^2 - 5y_B^3}{144(1 - y_B)^3} + \frac{y_B^2}{8(1 - y_B)^4} \log y_B, \quad (97)$$

$$\xi_B^H(w_B) = -\frac{16w_B - 29w_B^2 + 7w_B^3}{144(1 - w_B)^3} + \frac{-2w_B + 3w_B^2}{24(1 - w_B)^4} \log w_B, \quad (98)$$

where we have approximated  $y_s = 0$ ,  $y_b = 0$  and  $m_s/m_b = 0$ .

## C Statistical analysis of observables with theoretical uncertainty

The most common situation when comparing a theoretical prediction  $x_t$  with an experimental measurement  $x_e$  is that the uncertainty in the former can be ignored. This does not happen for some observables analysed in this article, which are subject to low energy QCD uncertainties. For example, if we have for  $\varepsilon$   $x_e = (2.282 \pm 0.017) \times 10^{-3}$

and  $x_t = (2.42 \pm 0.42) \times 10^{-3}$ , how many standard deviations is  $x_t$  from  $x_e$ ? To answer naively that it is at  $8.1\sigma$  is clearly wrong, and the comparison between both should weigh in some way the error on  $x_t$ . Here we explain how we obtain in such cases a reasonable estimate of the agreement between the theoretical and experimental data.

Let us recall how  $x_e$  and  $x_t$  are compared when the former has a Gaussian distribution with mean  $\mu_e$  and standard deviation  $\sigma_e$  and  $x_t$  is error-free and equals  $\mu_t$  (see for instance Ref. [113]). The  $\chi^2$  value is defined as

$$\chi^2 = \left( \frac{\mu_e - \mu_t}{\sigma_e} \right)^2, \quad (99)$$

and from it the  $P$  number is computed as

$$P = \int_{\chi^2}^{\infty} f(z; 1) dz, \quad (100)$$

where  $f(z; n)$  is the  $\chi^2$  distribution function for  $n$  degrees of freedom,

$$f(z; n) = \frac{z^{n/2-1} e^{-z/2}}{2^{n/2} \Gamma(n/2)}. \quad (101)$$

The  $P$  value is the probability to obtain experimentally a  $\chi^2$  equal or worse than the actual one, that is, a result equal or less compatible with the theory. Performing the integral in Eq. (100),

$$P = 1 - \operatorname{erf} \sqrt{\frac{\chi^2}{2}} = 1 - \operatorname{erf} \frac{|\mu_e - \mu_t|}{\sqrt{2} \sigma_e}, \quad (102)$$

with erf the well-known error function. The probability to obtain an equal or better result is  $1 - P$ . For instance, with  $|\mu_e - \mu_t| = \sigma_e$  we have  $1 - P = \operatorname{erf}(1/\sqrt{2}) = 0.68$ , corresponding to one Gaussian standard deviation, as it obviously must be.

When  $x_t$  is not considered as a fixed quantity  $\mu_t$  but has some distribution function  $g(x_t)$  (that may be Gaussian or may not), we use the probability law  $P(A) = \sum_i P(A|B_i)P(B_i)$ , with  $\sum_i P(B_i) = 1$ , to convolute the  $x_t$ -dependent  $P$  number with  $g$ :

$$P = \int_{-\infty}^{+\infty} P|_{\mu_t \rightarrow x_t} g(x_t) dx_t = 1 - \int_{-\infty}^{+\infty} \operatorname{erf} \frac{|\mu_e - x_t|}{\sqrt{2} \sigma_e} g(x_t) dx_t. \quad (103)$$

The assumption that  $x_t = \mu_t$  without error can be translated to Eq. (103) choosing the “distribution function”  $g(x_t) = \delta(x_t - \mu_t)$ , in which case we recover Eq. (102).

An adequate (but not unique) choice of the function  $g(x_t)$  may be a Gaussian. One source of systematic uncertainties is often due to the input parameters involved in the

theoretical calculation ( $m_t$ ,  $\alpha_s$ , CKM mixing angles, etc.), whose experimental values are given by a Gaussian distribution. It is then likely that the distribution function  $g(x_t)$  (where  $x_t$  is also a function of its input parameters) has a maximum at  $\mu_t$  and falls quickly for increasing  $|x_t - \mu_t|$ . This feature can be implemented in a simple way by choosing  $g(x_t)$  as Gaussian, and we expect that the results are not very sensitive to the precise shape of the function  $g(x_t)$ .

Let us then assume that  $g(x_t)$  is a Gaussian with mean  $\mu_t$  and standard deviation  $\sigma_t$ . Intuitively, we expect that if  $\sigma_t \ll \sigma_e$ , Eq. (103) should reduce to Eq. (102). This is easy to show. Writing the explicit form of  $g(x_t)$ ,

$$P = 1 - \int_{-\infty}^{+\infty} \operatorname{erf} \frac{|\mu_e - x_t|}{\sqrt{2} \sigma_e} \frac{e^{-\frac{(x_t - \mu_t)^2}{2\sigma_t^2}}}{\sqrt{2\pi}\sigma_t} dx_t. \quad (104)$$

The limits of this integral can be taken as  $\mu_t - n\sigma_t$ ,  $\mu_t + n\sigma_t$ , with  $n \geq 4$ . The integral is negligible out of these limits due to the exponential (the error function takes values between 0 and 1). Changing variables to  $\Delta_t = x_t - \mu_t$ , we observe that  $|\Delta_t| \ll \sigma_e$  under the assumption that  $\sigma_t \ll \sigma_e$ . Expanding the error function in a Taylor series to order  $\Delta_t$ , the integral can be done analytically,

$$P = 1 - \operatorname{erf} \frac{n}{\sqrt{2}} \operatorname{erf} \frac{|\mu_e - \mu_t|}{\sqrt{2} \sigma_e}. \quad (105)$$

For  $n \geq 4$ ,  $\operatorname{erf} n/\sqrt{2} \simeq 1$  to an excellent approximation and we obtain Eq. (102), as we wanted to prove.

Results for  $P$  values can be expressed in a more intuitive form as standard “number of sigma”  $n_\sigma$  inverting Eq. (102),

$$n_\sigma = \sqrt{2} \operatorname{erf}^{-1}(1 - P), \quad (106)$$

with  $\operatorname{erf}^{-1}$  the inverse of the error function. However, this  $n_\sigma$  does not retain the geometrical interpretation of the distance between  $\mu_e$  and  $\mu_t$  in units of  $\sigma_e$  that has when  $\sigma_t \sim 0$ .

We apply this procedure to the example at the beginning of this Appendix, with  $x_e = (2.282 \pm 0.017) \times 10^{-3}$  and  $x_t = (2.42 \pm 0.42) \times 10^{-3}$ . Assuming for simplicity that the distribution of  $x_t$  is Gaussian, we obtain the much more reasonable result of  $n_\sigma = 2.25$ . This number must be compared with  $n_\sigma = 8.1$ , obtained without taking into account the theoretical error, *i. e.* calculating naively  $(\mu_t - \mu_e)/\sigma_e$ . The use of the theoretical error in the statistical comparison mitigates the discrepancy and implements

numerically, in a simple but effective way, what one would intuitively expect in this case. The result  $n_\sigma = 2.25$  reflects the fact that the theoretical and experimental values can have a good agreement if  $x_t$  is smaller than its predicted value  $\mu_t = 2.42 \times 10^{-3}$  but a bad one if  $x_t$  is larger, what is also possible because the theoretical error is of either sign. The prescription presented here has also one very gratifying property: if we change  $\mu_t \rightarrow \mu'_t = \mu_t + \delta\mu_t$ , with  $\delta\mu_t \ll \sigma_t$ , the  $P$  value is hardly affected. For  $\mu'_t = 2.35 \times 10^{-3}$ ,  $n_\sigma$  changes only to 2.23, while the pull calculated naively decreases to 4.

This construction can be generalised when not all the range of variation of  $x_e, x_t$  is physically allowed. We write without proof the expression for  $P$  in this case. Assuming that the physical region is  $x_e \geq 0, x_t \geq 0$ ,

$$P = 1 - \left[ 1 + \operatorname{erf} \frac{\mu_e}{\sqrt{2}\sigma_e} \right]^{-1} \times \int_0^\infty \left( \operatorname{erf} \frac{|\mu_e - x_t|}{\sqrt{2}\sigma_e} + \operatorname{erf} \frac{\max\{\mu_e, |\mu_e - x_t|\}}{\sqrt{2}\sigma_e} \right) g(x_t) dx_t. \quad (107)$$

Finally, notice that the expressions in Eqs. (103,107) for the  $P$  number are not symmetric under the interchange of theoretical and experimental data, even if  $g(\mu_t)$  is Gaussian. This reflects the fact that  $P(\text{data}|\text{theory}) \neq P(\text{theory}|\text{data})$ , but they are related by Bayes' theorem.

## Acknowledgements

I thank F. del Águila, R. González Felipe, F. Joaquim, J. Prades, J. Santiago and J. P. Silva for useful comments. I also thank J. P. Silva, F. del Águila, A. Teixeira and G. C. Branco for reading the manuscript. This work has been supported by the European Community's Human Potential Programme under contract HTRN-CT-2000-00149 Physics at Colliders and by FCT through project CERN/FIS/43793/2001.

## References

- [1] D. Abbaneo *et al.* [ALEPH Collaboration], hep-ex/0112021
- [2] M. Martínez, R. Miquel, L. Rolandi and R. Tenchini, Rev. Mod. Phys. **71**, 575 (1999)

- [3] A. Lai *et al.* [NA48 Collaboration], Eur. Phys. J. **C22**, 231 (2001)
- [4] R. Kessler, hep-ex/0110020.
- [5] K. Hagiwara *et al.*, Particle Data Group, Phys. Rev. **D66**, 010001 (2002)
- [6] T. Affolder *et al.* [CDF Collaboration], Phys. Rev. Lett. **86**, 3233 (2001)
- [7] Y. Nir and H. R. Quinn, Ann. Rev. Nucl. Part. Sci. **42**, 211 (1992)
- [8] Y. Nir, hep-ph/0109090
- [9] T. Higuchi [Belle Collaboration], hep-ex/0205020
- [10] B. Aubert *et al.* [BABAR Collaboration], hep-ex/0207042
- [11] M. Beneke *et al.*, hep-ph/0003033
- [12] J. A. Aguilar-Saavedra *et al.* [ECFA/DESY LC Physics Working Group Collaboration], hep-ph/0106315
- [13] T. Stelzer, Z. Sullivan and S. Willenbrock, Phys. Rev. **D58**, 094021 (1998)
- [14] A. S. Belyaev, E. E. Boos and L. V. Dudko, Phys. Rev. **D59**, 075001 (1999)
- [15] T. Tait and C.P. Yuan, Phys. Rev. **D63**, 014018 (2001)
- [16] F. del Aguila and J. A. Aguilar-Saavedra, Phys. Rev. **D67**, 014009 (2003)
- [17] F. del Aguila and M. J. Bowick, Nucl. Phys. **B224**, 107 (1983)
- [18] G. C. Branco and L. Lavoura, Nucl. Phys. **B278**, 738 (1986)
- [19] P. Langacker and D. London, Phys. Rev. **D38**, 886 (1988)
- [20] D. London, hep-ph/9303290
- [21] R. Barbieri and L. J. Hall, Nucl. Phys. **B319**, 1 (1989)
- [22] J. L. Hewett and T. G. Rizzo, Phys. Rept. **183**, 193 (1989)
- [23] Y. Nir and D. J. Silverman, Phys. Rev. **D42**, 1477 (1990)
- [24] E. Nardi, E. Roulet and D. Tommasini, Nucl. Phys. **B386**, 239 (1992)
- [25] V. D. Barger, M. S. Berger and R. J. Phillips, Phys. Rev. **D52**, 1663 (1995)

- [26] P. H. Frampton, P. Q. Hung and M. Sher, Phys. Rept. **330**, 263 (2000)
- [27] M. B. Popovic and E. H. Simmons, Phys. Rev. **D62**, 035002 (2000)
- [28] G. C. Branco, T. Morozumi, P. A. Parada and M. N. Rebelo, Phys. Rev. **D48**, 1167 (1993)
- [29] F. del Aguila, J. A. Aguilar-Saavedra and G. C. Branco, Nucl. Phys. **B510**, 39 (1998)
- [30] G. Barenboim, F. J. Botella, G. C. Branco and O. Vives, Phys. Lett. **B422**, 277 (1998)
- [31] K. Higuchi and K. Yamamoto, Phys. Rev. **D62**, 073005 (2000)
- [32] J. L. Rosner, Comments Nucl. Part. Phys. **15**, 195 (1986)
- [33] J. L. Rosner, Phys. Rev. **D61**, 097303 (2000)
- [34] J. D. Bjorken, S. Pakvasa and S. F. Tuan, Phys. Rev. **D66**, 053008 (2002)
- [35] F. del Aguila and J. Santiago, JHEP **0203**, 010 (2002)
- [36] G. Barenboim, F. J. Botella and O. Vives, Nucl. Phys. **B613**, 285 (2001)
- [37] D. Hawkins and D. Silverman, Phys. Rev. **D66**, 016008 (2002)
- [38] T. Yanir, JHEP **0206**, 044 (2002)
- [39] F. del Aguila, J. A. Aguilar-Saavedra and R. Miquel, Phys. Rev. Lett. **82**, 1628 (1999)
- [40] L. Lavoura and J. P. Silva, Phys. Rev. **D47**, 1117 (1993)
- [41] F. Abe *et al.* [CDF Collaboration], Phys. Rev. Lett. **80**, 2525 (1998)
- [42] G. Abbiendi *et al.* [OPAL Collaboration], Phys. Lett. **B521**, 181 (2001)
- [43] J. A. Aguilar-Saavedra and B. M. Nobre, Phys. Lett. **B553**, 251 (2003)
- [44] A. A. Akhundov, D. Y. Bardin and T. Riemann, Nucl. Phys. **B276**, 1 (1986)
- [45] J. Bernabeu, A. Pich and A. Santamaria, Nucl. Phys. **B363**, 326 (1991)
- [46] J. Bernabeu, A. Pich and A. Santamaria, Phys. Lett. **B200**, 569 (1988)

- [47] P. Bamert, C. P. Burgess, J. M. Cline, D. London and E. Nardi, Phys. Rev. **D54**, 4275 (1996)
- [48] D. Comelli and J. P. Silva, Phys. Rev. **D54**, 1176 (1996)
- [49] P. Abreu *et al.* [DELPHI Collaboration], Eur. Phys. J. **C14**, 613 (2000)
- [50] M. E. Peskin and T. Takeuchi, Phys. Rev. Lett. **65**, 964 (1990); Phys. Rev. **D46**, 381 (1992)
- [51] D. C. Kennedy and P. Langacker, Phys. Rev. Lett. **65**, 2967 (1990) [Erratum-ibid. **66**, 395 (1991)]; Phys. Rev. **D44**, 1591 (1991)
- [52] G. Bhattacharyya, S. Banerjee and P. Roy, Phys. Rev. **D45**, 729 (1992) [Erratum-ibid. **D46**, 3215 (1992)]
- [53] L. Lavoura and J. P. Silva, Phys. Rev. **D47**, 2046 (1993)
- [54] G. Barenboim and F. J. Botella, Phys. Lett. **B433**, 385 (1998)
- [55] M. Aoki, G. C. Cho, M. Nagashima and N. Oshimo, Phys. Rev. **D64**, 117305 (2001)
- [56] T. Inami and C. S. Lim, Prog. Theor. Phys. **65**, 297 (1981) [Erratum-ibid. **65**, 1772 (1981)]
- [57] G. Buchalla, A. J. Buras and M. E. Lautenbacher, Rev. Mod. Phys. **68**, 1125 (1996)
- [58] A. J. Buras, M. Jamin and P. H. Weisz, Nucl. Phys. **B347**, 491 (1990)
- [59] F. J. Gilman and M. B. Wise, Phys. Rev. **D27**, 1128 (1983)
- [60] L. Lellouch, Nucl. Phys. Proc. Suppl. **94**, 142 (2001)
- [61] S. Herrlich and U. Nierste, Nucl. Phys. **B476**, 27 (1996)
- [62] G. C. Branco, L. Lavoura and J. P. Silva, “*CP violation*”, Oxford University Press, 1999
- [63] C. T. Sachrajda, hep-lat/0101003
- [64] Y. Nir, talk at ICHEP 2002, Amsterdam, July 24–31, 2002



- [65] G. Eyal and Y. Nir, JHEP **9909**, 013 (1999)
- [66] K. Niyogi and A. Datta, Phys. Rev. **D20**, 2441 (1979)
- [67] A. Datta and D. Kumbhakar, Z. Phys. **C27**, 515 (1985)
- [68] A. A. Petrov, Phys. Rev. **D56**, 1685 (1997)
- [69] J. F. Donoghue, E. Golowich, B. R. Holstein and J. Trampetic, Phys. Rev. **D33**, 179 (1986)
- [70] G. C. Branco, P. A. Parada and M. N. Rebelo, Phys. Rev. **D52**, 4217 (1995)
- [71] C. Bernard *et al.* [MILC Collaboration], hep-lat/0206016
- [72] K. S. Babu, X. G. He, X. Li and S. Pakvasa, Phys. Lett. **B205**, 540 (1988)
- [73] W. J. Marciano and Z. Parsa, Phys. Rev. **D53**, 1 (1996)
- [74] G. Buchalla and A. J. Buras, Nucl. Phys. **B548**, 309 (1999)
- [75] G. Buchalla and A. J. Buras, Nucl. Phys. **B400**, 225 (1993)
- [76] S. Adler *et al.* [E787 Collaboration], Phys. Rev. Lett. **88**, 041803 (2002)
- [77] A. J. Buras and L. Silvestrini, Nucl. Phys. **B546**, 299 (1999)
- [78] D. Ambrose *et al.* [E871 Collaboration], Phys. Rev. Lett. **84**, 1389 (2000)
- [79] G. Valencia, Nucl. Phys. **B517**, 339 (1998)
- [80] G. D'Ambrosio, G. Isidori and J. Portoles, Phys. Lett. **B423**, 385 (1998)
- [81] C. H. Chang, D. Chang and W. Y. Keung, Phys. Rev. **D61**, 053007 (2000)
- [82] M. Aoki, E. Asakawa, M. Nagashima, N. Oshimo and A. Sugamoto, Phys. Lett. **B487**, 321 (2000)
- [83] A. J. Buras and R. Fleischer, Adv. Ser. Direct. High Energy Phys. **15**, 65 (1998)
- [84] K. G. Chetyrkin, M. Misiak and M. Munz, Phys. Lett. **B400**, 206 (1997)  
[Erratum-ibid. **B425**, 414 (1998)]
- [85] M. S. Alam *et al.* [CLEO Collaboration], Phys. Rev. Lett. **74**, 2885 (1995)

- [86] R. Barate *et al.* [ALEPH Collaboration], Phys. Lett. **B429**, 169 (1998)
- [87] S. Chen *et al.* [CLEO Collaboration], Phys. Rev. Lett. **87**, 251807 (2001)
- [88] B. Grinstein, M. J. Savage and M. B. Wise, Nucl. Phys. **B319**, 271 (1989)
- [89] G. Buchalla, G. Hiller and G. Isidori, Phys. Rev. **D63**, 014015 (2001)
- [90] K. Senyo [Belle Collaboration], hep-ex/0207005
- [91] A. J. Buras and M. Munz, Phys. Rev. **D52**, 186 (1995)
- [92] A. J. Buras, hep-ph/0101336
- [93] E. Pallante and A. Pich, Phys. Rev. Lett. **84**, 2568 (2000)
- [94] E. Pallante, A. Pich and I. Scimemi, Nucl. Phys. **B617**, 441 (2001)
- [95] J. Bijnens and J. Prades, Nucl. Phys. Proc. Suppl. **96**, 354 (2001)
- [96] A. Alavi-Harati *et al.* [E799-II/KTeV Collaboration], Phys. Rev. **D61**, 072006 (2000)
- [97] Y. Grossman and Y. Nir, Phys. Lett. **B398**, 163 (1997)
- [98] R. Fleischer and I. Dunietz, Phys. Rev. **D55**, 259 (1997)
- [99] Y. Nir and D. J. Silverman, Nucl. Phys. **B345**, 301 (1990)
- [100] I. Dunietz, R. Fleischer and U. Nierste, Phys. Rev. **D63**, 114015 (2001)
- [101] A. S. Dighe, I. Dunietz, H. J. Lipkin and J. L. Rosner, Phys. Lett. **B369**, 144 (1996)
- [102] I. Dunietz, Phys. Rev. **D52**, 3048 (1995)
- [103] G. Eilam, J. L. Hewett and A. Soni, Phys. Rev. **D44**, 1473 (1991) [Erratum-ibid. **D 59**, 039901 (1999)]
- [104] T. Han, R. D. Peccei and X. Zhang, Nucl. Phys. **B454**, 527 (1995)
- [105] F. del Aguila, J. A. Aguilar-Saavedra and Ll. Ametller, Phys. Lett. **B462**, 310 (1999)
- [106] F. del Aguila and J. A. Aguilar-Saavedra, Nucl. Phys. **B576**, 56 (2000)

- [107] T. Han and J. L. Hewett, Phys. Rev. **D60**, 074015 (1999)
- [108] S. Bar-Shalom and J. Wudka, Phys. Rev. **D60**, 094016 (1999)
- [109] J. A. Aguilar-Saavedra, Phys. Lett. **B502**, 115 (2001)
- [110] J. J. Cao, Z. H. Xiong and J. M. Yang, Nucl. Phys. **B651**, 87 (2003)
- [111] S. H. Kettell, hep-ex/0207044
- [112] H. Fusaoka and Y. Koide, Phys. Rev. **D57**, 3986 (1998)
- [113] G. Cowan, *“Statistical data analysis”*, Oxford University Press, 1998